Challenges and advances in the application of dynamic nuclear polarization to liquid-state samples

Nandita Abhyankar[1,2,*], **Veronika Szalai**[2,*]

[1]Institute for Research in Electronics and Applied Physics, University of Maryland, College Park, MD 20742, USA

[2]National Institute of Standards and Technology, Gaithersburg, MD 20899, USA

Abstract

Nuclear magnetic resonance (NMR) spectroscopy is a powerful method to study structure and dynamics of materials. The inherently low sensitivity of NMR spectroscopy is a consequence of low spin polarization. Hyperpolarization of a spin ensemble is defined as a population difference between spin states that far exceeds what is expected from the Boltzmann distribution for a given temperature. Dynamic nuclear polarization (DNP) can overcome the relatively low sensitivity of NMR spectroscopy by using a paramagnetic matrix to hyperpolarize a nuclear spin ensemble. Application of DNP NMR can result in sensitivity gains of up to four orders of magnitude compared to NMR without DNP. Although DNP NMR is now more routinely available for solid-state NMR spectroscopy, it has not been exploited to the same degree for liquid-state samples. This review will consider challenges and advances in the application of DNP NMR to liquid-state samples. The review is organized into four sections: (i) mechanisms of DNP NMR relevant to hyperpolarization of liquid samples; (ii) applications of liquid-state DNP NMR; (iii) available detection schemes for liquid-state samples; and (iv) instrumental challenges and outlook for liquid-state DNP NMR.

Graphical Abstract

*Corresponding authors: nandita.abhyankar@nist.gov, vszalai@nist.gov.
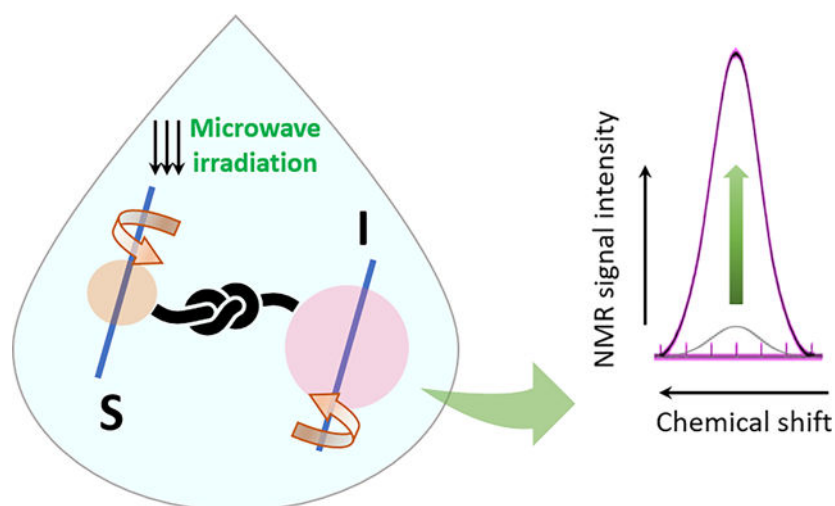
Introduction:

Nuclear magnetic resonance transitions have small energy scales ($E << kT$; where E is the energy difference between magnetic energy levels, k is the Boltzmann constant, and T is temperature of the system). Due to unfavorable Boltzmann factors ($N_{I = +1/2}/N_{I = -1/2} \approx 0.999999$ for an ensemble of proton nuclear spins at 1 K and 1 T), nuclear spin ensembles have very low spin polarization. The resulting low sensitivity of this method hinders its application to samples with limited mass, volume, or concentration. Development of instrumentation for high-field and low-temperature NMR has greatly improved detection limits but nuclear spin polarization is low even under these demanding conditions. Apart from these so-called 'brute force' strategies to increase spin polarization, dynamic nuclear polarization (DNP) has gained significant attention in the past few decades. In DNP, polarization is transferred from an electron spin ensemble to a nuclear spin ensemble; the large difference in timescales of relaxation of electron spins and nuclear spins results in hyperpolarization of the nuclear spin ensemble. Compared to nuclear spin ensembles, electron spin ensembles have much higher polarization as a result of the thousand-fold or greater advantage provided by the higher gyromagnetic ratio of an electron compared to nuclei. Secondly, the relaxation processes of an electron spin ensemble are much faster than those of a nuclear spin ensemble. DNP exploits these disparities to transfer polarization from electrons to nuclei, resulting in hyperpolarization of the nuclear spin ensemble. Most notably, the combination of DNP with magic angle spinning (MAS) has resulted in phenomenal improvements in sensitivity for solid-state samples.[1] In contrast, DNP NMR in the liquid state has not been explored to the same extent, despite its potential utility in applications such as nuclear magnetic resonance imaging and high-resolution NMR spectroscopy of biological samples.

Solid-state magnetic resonance spectra are broadened by dipolar interactions, anisotropies of chemical shift, and in some cases, anisotropies of quadrupolar interactions. Motional averaging removes this broadening in liquid-state experiments, yielding high-resolution spectra that contain information about structure and dynamics of molecules in solution.

Liquid DNP NMR has the potential to provide information that is presently inaccessible, particularly regarding dynamic processes that only occur under physiological conditions or in the liquid state. Such processes include reaction mechanisms, kinetics, and evolving chemical profiles of complex mixtures. Imaging of tissues necessarily involves aqueous solutions and is typically performed at ambient temperature. Spectroscopy at physiological temperatures is also important for determination of structure-function relationships in biomacromolecules. The sensitivity gains obtained from DNP make it particularly applicable to the study of low-concentration, mass-limited samples, such as transient species in reactions and aggregation-prone biomacromolecules. Membrane proteins, for example, are extremely challenging to study because their concentration must be limited due to their tendency to aggregate. Recent progress in DNP NMR with magic angle spinning (MAS) has been highly impactful in protein structure studies by improving sensitivity as well as resolution. Lyophilized membrane proteins allow solid-state (ss) NMR to be conducted at ambient temperatures. However, the protocols for sample preparation for ss NMR are not well-defined.[2] Liquid DNP NMR is a more general approach suitable for a broad range of samples. It can provide information about dynamic processes such as conformational changes, protein-ligand interactions, and changes in solvation during structural transformations. Liquid DNP NMR has the most potential for impact in spatio-temporal studies which must necessarily be conducted in the liquid state and are hindered by the small concentrations of transient species -- e.g., studies of solvation dynamics, reaction kinetics, metabolite profiling, and imaging. Such studies would benefit greatly from the sensitivity gains provided by DNP NMR. Section II provides examples of the benefits of liquid DNP NMR for these fields.

Several comprehensive reviews of DNP NMR, especially under the high-field conditions of modern NMR, are available.[1,3,4,5] There are also more recent reviews of liquid-state NMR.[6,7,8] These reviews provide an understanding of the mechanistic aspects of DNP NMR and particular methodological developments. In this review, we aim to highlight how hyperpolarization through DNP can be employed to achieve sensitivity gains for liquid-state NMR spectroscopy. We will consider the current scope, applications, opportunities for development, and experimental challenges hindering widespread adoption of liquid-state DNP NMR spectroscopy as an analytical tool. In Section I, we provide a brief description of the mechanisms of liquid DNP NMR, including both solid-state and liquid-state mechanisms because both are applied for liquid DNP NMR. In section II, we discuss potential applications that are particularly suitable for liquid DNP NMR. In Section III, we review available detection schemes that exploit various mechanisms. Finally, in Section IV, we attempt to delineate the challenges associated with these detection schemes, and survey future research directions in the development of instrumentation for DNP NMR for liquid-state samples.

Section I: Mechanisms relevant to liquid DNP NMR.

We shall consider only mechanisms for steady-state or continuous-wave (CW) DNP of insulators since these are predominantly applied in present-day DNP NMR detection schemes. In CW DNP, microwaves are continuously applied to the sample containing the paramagnetic material, called the polarizing agent (PA), in order to saturate the electron

paramagnetic resonance (EPR) transition. Under optimal conditions defined by microwave frequency, magnetic field, and temperature, hyperpolarization of the nuclear spin ensemble results from the dynamic process of spin-lattice relaxation of the polarized electron spin ensemble, resulting in transfer of spin polarization from electrons to nuclei. Following this process, Fourier transform (FT) NMR is conducted on the hyperpolarized nuclear spin ensemble using pulse schema.

Of the CW mechanisms, only the Overhauser effect is directly applicable to solutions. Here we first provide a brief description of the Overhauser effect. We will also describe, albeit qualitatively, solid-state DNP mechanisms (solid effect, cross effect, and thermal mixing) since these can be exploited by conducting DNP in the frozen, solid state, followed by rapid melting/dissolution and detection of NMR in the liquid state. The reader is directed to papers that provide in-depth mathematical discussions of these mechanisms and their theoretical limits. Finally, we will briefly discuss why integrating DNP with high-field NMR is challenging.

Electron-nuclear coupling through the hyperfine interaction (HFI) is the basis of all DNP mechanisms. In the first step of CW DNP, an electron spin ensemble in a static magnetic field is irradiated with high-intensity microwaves to saturate its electron spin resonance (see Figure 2a), creating a non-equilibrium state. Coupling between an electron and nucleus is mediated by the hyperfine interaction (HFI), which can be composed of the isotropic (scalar) Fermi contact term and/or the anisotropic dipolar term. The spin Hamiltonian $\widehat{H}$ for a coupled two-spin (electron – nucleus, S = ½, I = ½) system is shown in the high-field limit, where the static field is applied in the z direction and all other terms can be treated as perturbations to the electron Zeeman term H_S:

$$\widehat{H} = \widehat{H}_S + \widehat{H}_I + \widehat{H}_{SI} = \omega_{0S}\widehat{S}_z - \omega_{0I}\widehat{I}_z + \widehat{A}_{SI}^{FC} + \widehat{A}_{SI}^{dip} \qquad \text{(Eq. 1)}$$

where $\widehat{H}_S$ is electron Zeeman term, $\widehat{H}_I$ is the nuclear Zeeman term, $\widehat{H}_{SI}$ is the hyperfine term, ω_{0S} and ω_{0I} are the electron and nuclear Larmor frequencies respectively, $\widehat{S}_z$ and $\widehat{I}_z$ are the z-components of the electron and nuclear spin operators respectively, $\widehat{A}_{SI}^{FC}$ is the Fermi contact (scalar) part of the HFI (see Eq. 2 below) and $\widehat{A}_{SI}^{dip}$ is the distance-dependent, anisotropic dipolar part of the HFI (see Eq. 3 below).

$$\widehat{A}_{SI}^{FC} = \frac{\gamma_S\gamma_I\hbar^2 8\pi}{3}|\psi(0)|^2 \boldsymbol{I} \cdot \boldsymbol{S} \qquad \text{(Eq. 2)}$$

where γ_S and γ_I are the gyromagnetic ratios of the electron and proton respectively, and $\psi(0)$ is the electron spin density at the nucleus (s-electron density is the only contributor to this term).

$$\widehat{A}_{SI}^{dip} = \gamma_S\gamma_I\hbar^2 \left[\frac{\boldsymbol{I} \cdot \boldsymbol{S}}{r^3}\right] - \frac{3(\boldsymbol{I} \cdot \boldsymbol{r})(\boldsymbol{S} \cdot \boldsymbol{r})}{r^5} \qquad \text{(Eq. 3)}$$

Figure 2b shows the eigen level diagram and possible transitions in the coupled two-spin (electron-proton; S = ½, I = ½) system described above. Single-quantum (SQ) transitions are the allowed transitions in conventional perpendicular-mode EPR excitation (excitation field B_1 applied perpendicular to static field B_0). They are described by the selection rule $m_S = \pm 1$, $m_I = 0$. Double quantum (DQ) and zero quantum (ZQ) transitions involve simultaneous electron and nuclear spin flips and are forbidden. However, it is precisely these forbidden transitions that provide the cross-polarization pathways resulting in nuclear hyperpolarization. Selective driving of either the ZQ or DQ transition results in 'overpopulation' of the |–> or |+> nuclear state, respectively, resulting in a population difference much higher than that expected from the Boltzmann thermal distribution. Hyperpolarization through the ZQ transition overpopulates the lower nuclear energy level, resulting in positive enhancement of the NMR signal. Conversely, hyperpolarization through the DQ transition results in negative enhancement of the NMR signal.

It is evident from the above explanation that the success of DNP depends on two factors: first, increasing the probability of the forbidden ZQ or DQ transition and second, the ability to selectively drive either the ZQ or the DQ transition. The HFI can mediate these nominally forbidden transitions in two ways:

i. Random fluctuations in the hyperfine term can provide a cross-relaxation pathway to transfer polarization from the electron spin ensemble to the nuclear spin ensemble. This is the mechanism of DNP proposed originally by Overhauser for metals. In metals, electron delocalization causes random fluctuations of the electronic wave function, which results in cross-relaxation from the electron spin ensemble to the nuclear spin ensemble through the scalar part of the HFI.[10] In insulating liquids, these random fluctuations are provided by translational or rotational diffusion of molecules.[11] DNP enhancement of the NMR signal is maximized when the rate of fluctuation of the hyperfine term matches the frequency associated with the ZQ or DQ transition.

ii. The dipolar part of the HFI can result in mixing of nuclear states, allowing direct excitation of the nominally forbidden ZQ and DQ transitions. This is the basis of the 'solid effect', which describes DNP enhancement in insulating solids.[11]

Dipolar coupling can induce SQ, ZQ, and DQ transitions while scalar coupling induces ZQ transitions selectively.

Whereas the Overhauser effect and solid effect are two-spin mechanisms, the cross-effect and thermal mixing are three-spin mechanisms that may be thought of simplistically as cross-polarization through coupling of two different electron-nucleus systems sharing the same nucleus. Often, a combination of mechanisms is observed, with one being dominant depending on the choice of physical conditions, PA, and concentration of PA. The study of nuclear hyperpolarization mechanisms is an active field, with ongoing theoretical and experimental work to elucidate and quantify various factors that determine DNP enhancement. Below, we describe characteristics of the four main classes of DNP mechanisms relevant to liquid DNP NMR. We delineate the interactions responsible for transfer of polarization from electrons to nuclei, conditions for observing DNP, and how

DNP enhancement is affected by field strength for each mechanism. The Overhauser effect is described in greater detail while the solid effect, cross effect, and thermal mixing are described qualitatively. Theoretical work on solid-state mechanisms is ongoing and the interested reader is directed to papers describing these effects in greater detail.

1. Overhauser effect: This is the only mechanism that can result in direct DNP enhancement in the liquid state. Overhauser predicted that the spin polarization of a bath of conduction-electrons could be transferred to a nuclear spin ensemble. Spin polarization of the conduction-electron spin ensemble must first be saturated by irradiation with microwaves of frequency ω_0. Cross-relaxation through the Fermi contact term of the HFI (H_{SI}, Eq. 1) results in hyperpolarization.[10] This effect, which he thought would only apply to the case of metals, was verified experimentally by Carver and Slichter for metallic lithium.[12] Abragam pointed out the mechanisms by which Overhauser enhancement could be achieved for insulating solids and solutions.[11,13] In Overhauser DNP of paramagnetic ions in solution, electron-nuclear (e-n) cross-relaxation can occur through stochastic fluctuations of the dipolar and/or scalar parts of the HFI. Time-dependence of the dipolar part of the HFI in solutions may be associated with electron spin relaxation, electron spin exchange, chemical exchange, or translational/rotational motions. On the other hand, time-dependence of scalar interactions is typically associated with processes that change the electronic configuration and s-electron density of the paramagnetic species, including electron spin relaxation, electron spin exchange, and chemical exchange.[9]

Under the condition that electron spins relax much faster than nuclear spins, Solomon described the enhancement in steady-state nuclear spin polarization as:[14]

$$\frac{\langle I_z \rangle}{I_0} = 1 + \left(\frac{w_2 - w_0}{w_0 + 2w_I + w_2} \right) \left(\frac{w_0 + 2w_1 + w_2}{w_0 + 2w_1 + w_2 + w^0} \right) \left(\frac{\langle S_0 \rangle - \langle S_z \rangle}{\langle S_0 \rangle} \right) \qquad \text{(Eq. 4)}$$

Here, w_0 and w_2 represent the transition rates for the ZQ and DQ transitions respectively. w_I represents the rate of the single quantum nuclear transition ($I = \pm 1, \quad S = 0$) while w_0 represents the rate of nuclear spin relaxation through all other means besides electron-nuclear coupling.

Eq. 4 may be rewritten as Eq. 5 to define the factors that determine DNP enhancement via the Overhauser effect.

$$\varepsilon = 1 - \xi f s \frac{\gamma_S}{\gamma_I} \qquad \text{(Eq. 5)}$$

where

$$\xi = \frac{w_2 - w_0}{w_0 + 2w_N + w_2} \qquad \text{(Eq. 6)}$$

$$f = \frac{w_0 + 2w_1 + w_2}{w_0 + 2w_1 + w_2 + w^0} \qquad \text{(Eq. 7)}$$

$$s = \frac{\langle S_0 \rangle - \langle S_z \rangle}{\langle S_0 \rangle} \qquad \text{(Eq. 8)}$$

The enhancement of nuclear spin polarization, $\varepsilon = \frac{\langle I_z \rangle}{I_0}$, is then a function of three factors:

(i) the coupling factor, ξ, which is the ratio of polarization enhancement through selectivity of the DQ or ZQ transition over relaxation through all other competing transitions; (ii) the leakage factor, f, which describes how much of nuclear relaxation is caused by coupling to the electron spin (when $f = 1$, nuclear spin relaxation is exclusively through coupling to the electron spin and when $f = 0$, electron-nuclear coupling does not contribute to nuclear spin relaxation); and (iii) the saturation factor, s, which describes how completely the electron spin resonance transition can be saturated.

As mentioned earlier, enhancements from DQ transitions offset those from ZQ transitions. Eq. 6 indicates that the enhancement factor increases as the rates of DQ and ZQ transitions become well separated so that one can be driven selectively over the other. DQ transitions result in positive enhancement of nuclear polarization while ZQ transitions result in negative enhancement. Enhancement factors on the order of 10^4-10^5 have been reported for liquid-state samples.[15]

Decrease in ODNP enhancement at high fields.: The DNP enhancement depends on the coupling factor (Eq. 6), which in turn is a function of the transition rates for the DQ, ZQ, and nuclear single-quantum transitions. In liquids, HFI may be modulated by stochastic fluctuations of the dipolar HFI, scalar HFI, or a mixture of both. As mentioned above, time-dependence of the dipolar HFI may be associated with relaxation and exchange of the electron spin, chemical exchange, as well as rotational and translational diffusion. On the other hand, time-dependence of the scalar HFI can only be a result of electron spin relaxation, electron spin exchange or chemical exchange. The spectral density functions $j_d(\omega)$ and $j_s(\omega)$ describe the match between the ZQ/DQ transition frequencies and the modulation frequency of the HFI. The coupling factor for a system with a mixture of dipolar and scalar HFI can be described in terms of the spectral density functions:[9]

$$\xi = \frac{M_d j_{d2}(\omega_s) - M_s \frac{\tau_{s2}}{\tau_{d2}} j_{s2}(\omega_s)}{M_d \left\{ \frac{7}{5} j_{d2}(\omega_s) + \frac{3}{5} \frac{\tau_{d1}}{\tau_{d2}} j_{d1}(\omega_I) \right\} + M_s \left\{ \frac{\tau_{s2}}{\tau_{d2}} j_{s2}(\omega_s) + \beta \frac{\tau_{s1}}{\tau_{s2}} j_{s1}(\omega_I) \right\}} \qquad \text{(Eq. 9)}$$

Here, the subscripts *1* and *2* stand for longitudinal and transverse components as used in the Bloch formulation. M_d and M_s are the components of the mixing parameter M, which is the ratio of scalar to dipolar coupling. β describes the attenuation of the scalar enhancement due to spin exchange. It can range between 0 and 1, where $\beta = 0$ indicates no spin exchange.

The spectral density functions for time-dependence of the scalar and dipolar HFI are given by the following equations:

$$j_d(\omega) = \frac{1}{1 + \omega^2 \tau_d^2}$$

(Eq. 10)

and

$$j_s(\omega) = \frac{1}{1 + \omega^2 \tau_s^2}$$

(Eq. 11)

where ω is the frequency of the ZQ/DQ transition and τ is the correlation time for the associated HFI modulation. These equations indicate that when $\omega_s \gg 1/\tau$, the spectral density function for cross-relaxation becomes vanishingly small, with a corresponding decrease in the coupling factor. This describes the case at high fields, where the Zeeman splitting becomes much larger than the modulation frequency of the HFI, e.g., when molecular motions are no longer fast enough to facilitate the ZQ/DQ transitions. Similarly, in solids, the transverse fields provided by the electron-nuclear dipolar interaction are too small to allow mixing of nuclear energy levels at high fields. Therefore, DNP generally becomes less efficient at high fields.

Scalar enhancement occurs exclusively through the Fermi contact interaction. It is in principle independent of field and can allow DNP to be conducted at high fields.[6, 16] However, this situation is rarely observed because DNP enhancement in samples with a scalar HFI contribution is often attenuated by spin exchange processes ($\beta > 0$). Thus, the coupling factor can range from −1 to +0.5, where $\xi = +0.5$ indicates purely dipolar modulation of HFI and $\xi = -1$ indicates purely scalar modulation of HFI (Figure 1c).

2. Solid effect: Abragam described how DNP could occur in an insulating solid containing a small concentration of paramagnetic impurities.[11] In this case, hyperpolarization of the nuclear spin ensemble is achieved through direct excitation of DQ and ZQ transitions by microwave irradiation of frequency $\omega_{0S} \pm \omega_{0I}$. Dipolar electron-nuclear interactions cause a slight tilting of nuclear magnetic moments, resulting in energy level mixing that facilitates the nominally forbidden DQ and ZQ transitions. The degree of mixing is described in terms of the factor q, which describes the dipolar coupling between the electron and nucleus:

$$q = -\frac{3}{4} \frac{\gamma_S \gamma_I}{\omega_{0I}} \frac{1}{r^3} sin\theta cos\theta e^{-i\varphi}$$

(Eq. 12)

Microwave frequency ($\omega_{0S} - \omega_{0I}$) drives the DQ transition while ($\omega_{0S} + \omega_{0I}$) drives the ZQ transition (Table 1). As mentioned in the description of the Overhauser effect, driving the DQ transition results in positive enhancement while the ZQ transition results in negative enhancement. To ensure that these two enhancements do not cancel each other out, it is desirable to selectively drive one of the two forbidden transitions by fulfilling the condition that the EPR linewidth must be much smaller than ω_{0I}.

Field dependence of SE: As with the Overhauser effect, the solid effect also becomes less efficient at higher fields. At low to intermediate fields, the spin temperature and dipolar temperature become comparable.[11] The resulting quasi-continuous energy level distribution at low fields increases the efficiency of cross-relaxation between spin levels. In contrast, at high fields, spin temperature and dipolar temperature are well-separated in magnitude. Therefore, the solid effect becomes less efficient as the field is increased. The solid effect may also be observed in viscous liquids. For examples, the rotational correlation time of vanadyl complexes is slow enough to result in DNP enhancement through the solid effect while yielding liquid-state NMR spectra of protons, which have a much faster rotational correlation timescale.[17]

3.   Cross effect and thermal mixing: Other than the two-spin mechanisms described above, there are two other broad classes of mechanisms that are characterized by DNP enhancements that increase with the concentration of the paramagnetic material. Hwang and Hill reported a new hyperpolarization mechanism that is distinguishable from the solid effect because of the field profile of the enhancement factor (Table 1).[18] In this mechanism, the peaks in positive and negative enhancement become stronger and more well-resolved when the concentration of the paramagnetic dopant is increased (in contrast to the solid effect, which becomes less efficient at high concentrations of PA).

Hwang and Hill provided a phenomenological description of the cross effect (CE) for systems with high electron spin polarization.[19] CE relies on the presence of an EPR line that is inhomogeneously broadened by g-anisotropy. Such a system consists of multiple spin packets with varying ESR frequencies. Consider two spin packets, 'i' and ''i+1', that are dipolar-coupled, with allowed SQ EPR transition frequencies related by the expression $\omega_e^{i+1} = \omega_e^i + \omega_N$, where ω_N is the nuclear Larmor frequency of the nuclei that are dipolar-coupled to the electron spin packets. Since $\omega_e^i + \omega_N$ is the transition frequency of the ZQ transition for the spin packet *i*, this forbidden transition can now be cross coupled with the allowed SQ transition of the spin packet *i+1*, ω_e^{i+1} (Figure 1c). Similarly, ω_e^i is cross-coupled to the DQ transition of the spin packet *i−1*, where $\omega_e^i = \omega_e^{i-1} + \omega_N$. The resulting nuclear hyperpolarization through cross-coupling of the allowed EPR transition of one spin packet with the forbidden transition of another spin packet is termed the cross effect. For maximum efficiency of CE, the linewidth of the inhomogeneously broadened ESR line must be greater than the nuclear Larmor frequency. Because cross-coupling is possible with both DQ and ZQ transitions, lower net enhancements are observed due to offsetting of positive enhancements by negative enhancements.

Thermal mixing: Thermal mixing (TM) is also a three-spin process and is the dominant mechanism of hyperpolarization at high concentrations of PA. TM requires high fields and ultralow temperatures (< 4K), and is observed in the presence of PAs that appear to have homogeneously broadened lines at low or intermediate fields but with appreciable g-factor dispersion at high fields. Unlike CE (which can only yield polarization transfer between nuclei with the same gyromagnetic ratio), TM allows transfer of polarization between nuclear ensembles of different gyromagnetic ratios, e.g. [1]H and [13]C. This transfer of polarization is mediated by energy transfer between different thermal spin

reservoirs via dipolar interactions (Figure 1c). The first mathematical description was provided by Borghini,[20] and a more generalized mathematical description was provided by Wenckebach.[21] First, the ESR transition is saturated at frequency ω_{0S}. The central assumption in the thermal mixing mechanism is that the electron spin polarization is transferred throughout the entire EPR spectrum via spin diffusion, on a timescale that is much faster than any other relaxation process. This polarization is then transferred to the nuclear spin reservoir through the HFI, resulting in nuclear hyperpolarization.[21]

Field-dependence of CE and TM: Cross-coupling between spin packets becomes less efficient at higher fields because it becomes increasingly difficult to satisfy the condition $\omega_S > \omega_N$. Thus, both the CE and TM enhancements scale with $1/B_0$.

The study of solid-state nuclear hyperpolarization mechanisms is an active field, with ongoing theoretical and experimental work to elucidate and quantify various factors that determine DNP enhancement.[22–24] The dominant mechanism in a DNP experiment is affected by a complex interplay of experimental conditions, including temperature, field, frequency, and concentration of PA.[25] In the solid state, more than one mechanism may be operational simultaneously. For example, as the concentration of PA is increased, the SE becomes less efficient and the CE or TM may take over. We have qualitatively described the origins of various mechanisms of DNP enhancement, focusing on CW mechanisms which are described in terms of macroscopic rates of relaxation via fluctuations of the scalar and dipolar HFI. However, we note that quantum mechanical models were developed early on,[26,27] and have also been proposed more recently for the case of EPR excitation using microwave pulses.[28–30]

Section II: Applications of liquid-state DNP NMR

The examples listed below and summarized in Figure 2 show that liquid-state DNP NMR has broad and fundamental applications ranging from studies of reaction kinetics and mechanisms, metabolomics, imaging/metabolic imaging, to structural studies of biomolecules. Liquid-state DNP NMR is also envisioned to have a profound impact on the future of quantitative NMR.[33] Here we note some areas where liquid-state DNP NMR has yielded or promises to yield unique, previously unavailable information.

➤ **Studying protein hydration:** Liquid-state NMR studies provide information about dynamics of solute-solvent interactions. For example, protein molecules are surrounded by a hydration layer, the dynamics and heterogeneity of which are thought to be a determinant of protein function.[34] Han *et al.* have conducted seminal work in the use of Overhauser DNP (ODNP) for selective probing of local or 'internal' water surrounding peptides and proteins in varied environments.[35–37] Using a combination of site-directed spin-labeling and ODNP, Han *et al.* separate signals of local water surrounding a protein from bulk aqueous solution. In this method, DNP occurs by transfer of electron spin polarization of spin labels attached at selected sites to protons of water molecules diffusing in the vicinity of the spin label. Translational diffusion of the water molecules modulates the dipolar interaction between the electron spin of the spin label and nuclear spins of the local water protons, and this modulation results in cross-polarization from the electron spins to the nuclear

spins through the Overhauser effect. Thus, ODNP isolates the translational dynamics of the hydration layer, occurring on the picosecond-to-nanosecond timescale. Secondly, ODNP selectively amplifies the signal from water molecules interacting with the site of interest, while separating out the background NMR signal of bulk water. More recently, the technique has been used by Segawa *et al.* to observe penetration of water into a model membrane and its interaction with a membrane-inserting peptide.[38] They found that ODNP was the only technique able to distinguish accessibility in a site-selective manner, validating the utility of ODNP in distinguishing areas of heterogeneity with single-residue resolution. Chaubey *et al.* observed changes in dynamics of the solvent 2,2,2-trifluoroethanol (TFE) when the peptide melittin undergoes structural reorganization from a random coil to a helical structure. They measured the DNP enhancement of ^{19}F by the polarizing agent TEMPOL, and used the DNP coupling parameter as an indicator of the correlation time of the co-solvent TFE.[39] Hyperpolarized water has also been used to measure protein hydration by increasing the sensitivity of techniques such as fast 2D NMR, exchange spectroscopy (EXSY), and nuclear Overhauser effect spectroscopy (NOESY).[40–43]

Studying membrane proteins, disordered proteins, and aggregation-prone biomacromolecular systems: Membrane proteins are a particularly suitable example of the type of aggregation-prone biomacromolecules that could benefit from improvements to liquid-state DNP NMR. The maturation of solid-state DNP NMR with MAS has yielded valuable high-resolution structural information about these systems.[44, 45] However, these proteins remain difficult to solubilize/reconstitute in active form.[2] Liquid DNP NMR can provide information about dynamics processes, such as changes in conformation and solvation, for a wide range of samples, including in-cell samples. An advantage of DNP NMR is that by using site-directed spin labeling, hyperpolarization can be achieved with high site-specificity, thus allowing highly localized probing of protein dynamics and secondary structure. Hilty *et al.* recently used the method of dissolution-DNP (d-DNP) to hyperpolarize lipids (dodecyl phosphocholine), and monitored lipid interactions with the membrane protein OmpX.[46] By exploiting the facile exchange of amide protons, hyperpolarized water has also been used to obtain high-resolution 2D NMR spectra of disordered proteins.[47] Hyperpolarized ligands have been used to selectively enhance signals of ligand-binding sites[48,49] or to transfer polarization to other nearby ligands[50] on the protein. A potential application of high-throughput, quantitative analysis of ligand-protein interactions using liquid-state DNP NMR is the screening of small-molecule ligands for drug development.[48,51] (High-throughput biochemical assays, typically based on fluorescence readout, are the workhorses to identify potential drug/target combinations; however, such assays do not provide the atomic-level structural details required for *in silico* methods for drug design and discovery.[52])

➢ **Observing transiently formed species in solution for reaction monitoring and mechanistic studies.**—Hyperpolarization amplifies the NMR signal so that single-scan pulse experiments with otherwise low sensitivity can now be used to track the progress of a reaction by monitoring temporal profiles of NMR spectra. This ability has been used to observe reaction intermediates, conduct mechanistic studies, and monitor reaction kinetics.

Hilty *et al.* have conducted extensive work on the use of hyperpolarized substrates for monitoring non-equilibrium reactions with second to sub-second resolution.[53,54] Recently, they used d-DNP-enhanced pulse NMR to monitor the styrene polymerization reaction and the reaction of *p*-anisaldehyde with isobutylamine, with second-scale resolution.[55] They were able to extract single-scan ^{1}H-^{13}C correlation spectra during the reaction and calculated ^{1}H chemical shifts from ^{13}C spectra of transient species, demonstrating direct observation of transient species formed during the reaction. Jensen and Meier used hyperpolarized fructose to identify a previously elusive reaction intermediate and to monitor the carbohydrate dehydration reaction.[56] There are many examples of the use of d-DNP to identify reaction intermediates and measure reaction kinetics of organic and inorganic reactions.[57–61]

Hyperpolarization has been similarly exploited to study kinetics of protein-enzyme/protein-ligand complex formation. ^{13}C NMR spectra provide signatures of protein-ligand binding, and the broad frequency dispersion of ^{13}C spectra overcomes the problem of potential chemical shift overlap encountered in proton NMR. However, ^{13}C NMR spectra are weaker than ^{1}H NMR spectra because of the lower gyromagnetic ratio of ^{13}C. DNP enhances the weak ^{13}C signals, and has been used for ligand binding studies, including enzymatic assays.[62] As with organic reactions, d-DNP has been used to increase the signal intensity of single-scan ^{13}C spectra collected when monitoring biochemical reactions, enabling acquisition of data points at sub-second intervals for more than a minute as the reaction progresses.[63–67] Hilty *et al.* have used DNP to obtain ^{13}C DNP NMR spectra of lipid membranes, characterizing their biosynthetic pathways based on fractional isotopic labeling of reactant feeds.[68] Duus *et al.* also used DNP of ^{13}C to study the mechanism and kinetics of transglycosylation.[69]

➤ **Metabolomics:** NMR of heteronuclei (nuclei other than ^{1}H, e.g. ^{13}C, ^{15}N etc.) is advantageous for metabolite profiling because the NMR signals of heteronuclei are dispersed over a large frequency range and also do not need to be separated from the large background signal of aqueous protons in cells. However, the low, shifting concentrations of metabolites along with the low natural abundances of NMR-active heteronuclei result in metabolite quantities that are undetectable by conventional NMR spectroscopy. Hyperpolarization can amplify the signal from these low-concentration metabolites and increase the speed of analysis by eliminating the need for signal averaging. The increased signal-to-noise ratio (SNR) and speed of data collection allow real-time detection and monitoring of metabolites for clinical and investigative purposes. This approach was first demonstrated by Thaning *et al.*, who injected ^{13}C-hyperpolarized pyruvate into rats, and subsequently detected, monitored, and quantified the metabolites lactate, hydrate, alanine, bicarbonate, and pyruvate at 3 s intervals for 50 s after injection.[70] Ardenkjær-Larsen *et al.* demonstrated the utility of ^{13}C d-DNP NMR to determine levels of the anticonvulsant carbamazepine and its major metabolite carbamazepine-10,11-epoxide in blood plasma.[71] Brindle *et al.* conducted *in vitro* and *in vivo* studies of ascorbic and dehydroascorbic acid hyperpolarized by d-DNP, using these as probes of tumor redox status (loosely understood as the balance of oxidants and anti-oxidants in cells).[72] The signal intensities of metabolites tracked in these reports indicate the suitability of DNP NMR for quantitative NMR.[73]

➤ **In-cell DNP NMR:** All the above-mentioned analyses, including reaction monitoring and metabolite analyses, can provide valuable information if conducted within a native cellular environment. Frydman *et al.* used d-DNP followed by magnetization transfer from ^{13}C to ^{1}H to monitor the actions of pyruvate decarboxylase and pyruvate formase lyase enzymes.[74] They were able to perform these experiments in both yeast and bacteria. Meier *et al.* observed acetate influx and subsequent metabolic consequences in yeast.[75] Meier *et al.* and Balbach *et al.* have presented comprehensive reviews of the applications of in-cell hyperpolarized NMR.[76, 77] It should be noted that solid-state in-cell DNP NMR is an emerging field.[78,79] However, only liquid-state DNP has the potential to provide information about dynamic processes such as conformational changes, reaction kinetics and evolution of metabolite profiles in intact cells.

➤ **Imaging/Metabolic imaging:** In addition to spectroscopic metabolite profiling, hyperpolarization also improves imaging of metabolites by amplifying their NMR signal.[70] ^{13}C-labeled pyruvate is the most commonly used molecular probe in metabolic imaging, which is expected to be highly impactful as a clinical tool because of the noninvasive nature of magnetic resonance techniques and non-toxicity of spin-probes,[80,81] many of which occur endogenously. Metabolic imaging of hyperpolarized pyruvate is expected to be useful for tracking redox status of tissues, oxidative stress, and profiling the effects of radiation.[82–84] Similar to the study by Thaning *et al.*, Ardenkjaer-Larsen *et al.* demonstrated the use of metabolic imaging to scan implanted tumors in rats and to quantify the glycolytic status of cancer cells.[85] Glycolysis has also been quantified by imaging of hyperpolarized ^{13}C-labeled glucose[86] and fructose.[87]

Hyperpolarization enhancements can be similarly used to image other types of spin probes and spin traps. ^{13}C-labeled spin traps have been used to image reactive oxygen species (ROS) in tumors, allowing quantification of the redox status of cancer cells. When the hyperpolarized spin-trap is injected into the tumor, it reacts with ROS to form diamagnetic adducts. Hyperpolarization allows detection of reaction intermediates, which is the origin of the measured signal prior to adduct formation.[88,89]

➤ **Increasing the sensitivity of alternative NMR methodologies and low-field NMR:** In NMR relaxometry, sample components are characterized by their magnetization decay profiles (due to spin-lattice relaxation or spin decoherence) as a function of field or frequency. This technique suffers from poor sensitivity and resolution at lower frequencies and in multi-component chemical systems. Hyperpolarization via a spin label can enhance the signal at low frequencies while also allowing observation of specific sites via DNP through spin labels. DNP enhanced NMR can be used as a complementary technique to relaxometry,[90] but DNP may also be used to enhance signals for relaxometry. Selective DNP-enhanced fast field cycling (FFC) relaxometry can be used to separate signals of protein and solvent[91] or to measure the properties of the composing polymers of a block copolymer in solution.[92] Finally, relaxometry profiles in the solution state can help to design ODNP material systems by predicting DNP enhancements.[93,94] Low-field NMR, which has particular applications in compact NMR and *in vivo* imaging, is another sub-field in which gains of more than a hundred-fold may be obtained by using DNP. Compact NMR

can enable 'on-field' measurements of low-concentration analytes, including hazardous substances and reaction intermediates.[95–97] Increasing the sensitivity of low-field magnetic resonance imaging would be highly beneficial for developing low-cost *in vivo* imaging instruments that do not require cryogens, which are increasingly scarce.[98,99]

Section III: Available detection schemes and challenges for liquid-state samples

Detection schemes: Of the DNP mechanisms discussed above, only the Overhauser effect is applicable directly to liquid-state samples. However, there are several experimental challenges associated with this mechanism, including lower efficiency at higher fields, solvent heating effects due to the high microwave power required to saturate the ESR transition, and lack of applicability to large molecules (this point is especially relevant for biomacromolecular samples). Low temperatures favor high enhancement factors, which is likely why early successes in detection schemes for liquid samples involved melting frozen solutions; hyperpolarization is achieved in the frozen, solid state at low or intermediate fields. The sample is then melted or rapidly dissolved in a hot solvent and transported to another high-field location, where NMR spectroscopy is conducted on the melted sample (or imaging conducted of the liquid sample injected into tissue). Such *ex situ* detection schemes have been highly successful for enhancing the NMR signals of liquid samples. Challenges associated with *ex situ* hyperpolarization are: (i) loss of polarization during transport and (ii) inability to average over multiple scans because sample preparation requires several hours and the sample is lost after one cycle due to dissolution in the hot solvent. On the other hand, *in situ* detection schemes eliminate the transport step, conduct DNP and NMR at the same field, and allow averaging over multiple scans. Prominent *ex situ* and *in situ* schemes are summarized below.

1.   *Ex situ* detection: As mentioned above, the experimental conditions (low temperatures and low-to-medium fields) that favor DNP are incompatible with those that are desirable for NMR spectroscopy of liquids (high fields that provide better sensitivity and resolution, and temperatures near room temperature). *Ex situ* methods overcome this incompatibility by separating the DNP and NMR steps so that each step is conducted under its respective optimal conditions. DNP is conducted in a separate location (either a separate magnet or the stray-field region of the NMR magnet) at lower fields and low temperature (in the frozen state). The hyperpolarized sample is then rapidly melted or dissolved in a hot solvent and transported to a separate high-field location where NMR spectroscopy is carried out. Here we label *ex situ* methods as all those in which there is a separation of locations for DNP and subsequent NMR detection. These locations may be separated by as little as a few cm or the sample may be transported to a completely different instrumental unit.

1.1.   *Dissolution DNP:* DNP (d-DNP)[15] is perhaps the most impactful hyperpolarization scheme implemented thus far, with commercial setups available (Hypersense by Oxford Instruments and SPINlab by GE Healthcare[†]) and several 'home-made' setups reported.[102–108]

[†]Certain commercial entities, equipment or materials may be identified in this document to describe an experimental procedure or concept adequately. Such identification is not intended to imply recommendation or endorsement by the National Institute of

Ardenkjær-Larsen *et al.* showed that hyperpolarization of a frozen solution (achieved via a solid-state mechanism i.e. solid effect, cross effect, or thermal mixing) is stable enough to be detected if the frozen solution is melted rapidly by dissolution in a hot solvent.[15] After the sample has been hyperpolarized, it is transported to a separate location for either spectroscopy[15] or imaging[109], provided the transport is accomplished more quickly than the relaxation of the sample polarization.

In d-DNP, hyperpolarization is carried out in the 'polarizer' (consisting of the magnet and cryostat) at a temperature of 1 K and static magnetic fields in the range of 3 T to 7 T. The optimal field for d-DNP depends on the relative relaxation times of nuclear and electron spin polarizations. Higher fields result in longer nuclear relaxation times while maintaining rapid electron-spin relaxation. Thus, d-DNP typically employs medium-to-high static magnetic fields, and future setups are projected to work with even higher fields.[110] A paramagnetic material with a narrow EPR line – typically a trityl or nitroxide radical – is dissolved in glycerol to a concentration of 10 mmol L^{-1} to 20 mmol L^{-1}. When frozen, this solution forms a glassy, homogeneously doped paramagnetic matrix that hyperpolarizes the nuclear spin ensemble of the sample. Hyperpolarization can also be achieved by first transferring polarization from unpaired electrons to protons, followed by cross-polarization to other low-γ nuclei, e.g. ^{1}H-^{13}C cross-polarization. A low-quality-factor (low-Q) metal cylinder is used to localize microwaves around the sample. Saddle coils fitted inside the metal cylinder are used to conduct solid-state NMR measurements of hyperpolarization while the sample is still in the polarizer. After hyperpolarization, superheated water is rapidly injected into the frozen glassy sample to convert it to an aqueous solution, which is transported out of the low-temperature region and either used for NMR spectroscopy at a higher field (> 9 T)[15] or injected into a tissue sample for imaging *in vitro* or *in vivo*.[109] The sample volume is typically around 100 μL and the volume of injected solvent is typically around 5 mL, resulting in dilution. Polarizations of 30 % to 90 % have been reported, translating to improvements of up to four orders of magnitude in the SNR, compared to NMR without DNP.

DNP requires high microwave powers in order to saturate the EPR transition. In d-DNP, high-power sources, such as gyrotrons with typical power outputs of approximately 200 mW are used to generate microwaves. Saturation of broad EPR lines can be improved by modulating the microwave frequency or field, which increases the fraction of DNP-active radicals.[111,112] Next, it is critical to transport the hyperpolarized sample to its destination without significant loss of polarization, which is exacerbated by the presence of the paramagnetic material acting as a relaxant of nuclear spin polarization. The transport step is automated so it can be accomplished within a few seconds.[113] Fields of a few tenths of a mT applied while transporting the sample are usually adequate to preserve polarization.[114]

d-DNP is most advantageous for inherently *ex situ* applications, e.g., it has been highly impactful by improving signals for *in vivo* imaging and it also enables real-time monitoring of metabolites.[70,86] However, it is limited by the long time – often several hours – required

to generate the hyperpolarized sample, which must then be transported and measured before the nuclear polarization relaxes. Widespread application of d-DNP in clinical settings requires that hyperpolarization be accomplished on large sample volumes (e.g. through high throughput) in a consistent and reproducible manner (quality control). To achieve these objectives, the following improvements have either been reported or are expected: (i) magnet design (incorporation of shielded magnets and dual-core magnets in the polarizer so that NMR spectroscopy can be conducted after short transport); (ii) development of optimized high-Q microwave resonators for greater saturation of the EPR transition; (iii) improvements in transport systems, e.g., the use of pneumatic systems to speed up transport from a timescale of several seconds to less than a second;[115] (iv) development of labile radicals or radical-free phases to eliminate paramagnetic species and extend the relaxation time of nuclear polarization; or formulation of persistent, transportable hyperpolarized states by manipulation of multi-phase systems.[116,117]

1.2.   Supercritical DNP: When Overhauser enhancement occurs through e-n cross-relaxation mediated by the dipolar component of the HFI, the frequency of modulation of the dipolar interaction must match the energy gaps associated with the forbidden transitions. These energy gaps increase at higher fields, and the correlation times must be correspondingly shorter to provide the required high-frequency modulation of the HFI. (This trend may not apply when the HFI is dominated by the scalar component, whose magnitude is independent of field.) Fast molecular motions in supercritical fluids result in correspondingly short correlation times and therefore, improved Overhauser enhancements.[16,118] Supercritical CO_2 can be obtained under relatively mild conditions – at room temperature and a pressure of approximately 7500 kPa. In supercritical DNP NMR, DNP is carried out at a lower field of 0.3 T. The supercritical solution is then transported to the high-field NMR magnet using a flow system.

Building on their work on flow-transfer NMR,[119–121] Dorn *et al.* have established the use of supercritical solvents for flow-transfer DNP NMR.[16] They use two protocols for flow DNP NMR: liquid-liquid intermolecular transfer (LLIT)[119] and solid-liquid intermolecular transfer (SLIT).[120,121] In the setup for LLIT, the solution is pumped from a high performance liquid chromatography (HPLC) unit, mixed with analytical grade CO_2 pumped from a superfluid chromatography unit (SFU), and equilibrated to a pressure of 17000 kPa (165 atm). The volume ratios of sample solution and CO_2 are determined by their relative flow rates. Thus, a 0.1 mL/min flow of sample solution and 1 mL/min flow of CO_2 at the time of mixing results in a 1:10 ratio of sample volume to supercritical CO_2 volume for hyperpolarization. The mixture is heated to 40 °C in a superfluid chromatography (SFC) oven, and the resulting supercritical fluid is directed to a low-field (0.33 T) magnet where hyperpolarization is carried out. Microwaves are generated by a klystron source, amplified, and localized at the sample volume using a TE102 cavity resonator. The hyperpolarized solution is then flowed to a high-field magnet for NMR spectroscopy. Here, radiowaves are localized at the sample volume using a Helmholtz detection coil. The typical sample volume is approximately 160 μL in the low-field magnet and approximately 60 μL in the high-field magnet.

The protocol for DNP NMR using SLIT is identical to the LLIT protocol, except that the sample flowing from the HPLC unit through the SFC oven does not contain the PA, i.e. nitroxide radicals. Nitroxide radicals immobilized on silica gel are placed in the 0.3 T magnet and hyperpolarization occurs as the supercritical solution flows over the silica gel. For benzene, Dorn *et al.* reported approximately 5-fold improvement of observed DNP enhancement in LLIT using supercritical CO_2 when compared to 'normal-flow' DNP NMR. SLIT DNP NMR with supercritical CO_2 showed a 10-fold improvement in observed DNP enhancement compared to normal-flow DNP NMR. In addition to better sensitivity, SLIT separates the PA from the sample and thus avoids the problem of paramagnetic relaxation during transfer from the low-field magnet to the high-field magnet. Finally, since the paramagnetic material is not mixed with the sample in the SLIT protocol, the sample can be recycled for multiple measurements.

Supercritical CO_2 has several desirable properties that make supercritical DNP a promising methodology, particularly for small-molecule analytes.[7,85] The polarity of supercritical CO_2 can be varied continuously by adding small volumes of co-solvents, making it suitable for polar as well as non-polar solutes. CO_2 is non-polar and thus avoids the dielectric heating effects observed in solvents like water. This is particularly important considering the high intensity of microwaves typically required for DNP. The use of CO_2 as a solvent yields a proton-free background. Most importantly, supercritical DNP gives the ability to achieve fast molecular tumbling, achieving correlation times of 2 ps to 5 ps at room temperature (compared to 5 ps to 6 ps at 400 K for water). These fast correlation times can enable Overhauser DNP at correspondingly higher fields/frequencies, making supercritical DNP an exciting prospect for enabling direct DNP enhancement in high-field NMR.

1.3.   Shuttle DNP: In shuttle DNP, the probe containing the liquid sample is shuttled between the low-field and high-field region produced by the same magnet, allowing separation of hyperpolarization and detection steps. Hyperpolarization occurs through Overhauser enhancement at low magnetic fields, after which the sample is shuttled to the high-field region for NMR detection. There are many early examples of the use of setups with multiple magnetic field regions in zero-field NMR, low-field NMR, NMR relaxation, and relaxation-dispersion measurements, which form the basis of the instrumental setups used in shuttle DNP.[122–124] In such setups, it is desirable to have several magnetic field regions either to separate the relaxation and detection steps or to study the field-dependence of relaxation time. Typically, the liquid sample is shuttled by a computerized pneumatic system over distances of 10 cm to 100 cm in times < 1 s. Fast and precise positioning at locations of specific field strengths in the fringe field of a magnet can be accomplished using stepper motors. Such setups have been used for fast field cycling NMR and the application has been extended to chemically-induced DNP (CIDNP) experiments.[125,126]

In the liquid state, there can be many reasons (besides inverse field-dependence of Overhauser enhancement) for choosing to conduct DNP at a lower field than that used for NMR detection. For example, Reese *et al.* chose to conduct hyperpolarization at the lower frequency of 10 GHz (0.3 T) because the larger wavelength allows higher sample sizes and decreased dielectric losses in an optimally designed cylindrical resonant cavity.[127] After DNP, the sample is shuttled downwards pneumatically to a 14 T magnet to take advantage of

the higher sensitivity and resolution of high-field NMR detection. This setup is not efficient for large molecules with fast proton relaxation times because hyperpolarization cannot be sustained through the drop in magnetic field during the shuttling step. In a variation of this setup, the low-field region is located in the stray field of the 14 T NMR magnet.[128] A ferromagnetic cylinder used for shimming provides a homogeneous-field length of 10 mm. By avoiding the drop in magnetization during a long transfer to a separate magnet, this setup extends the scope of shuttle DNP NMR to larger molecules.

2.   _In situ_ detection: Several ways have been proposed to overcome the problem of loss of polarization during sample transport, including two-center magnets and magnetic tubes. On the other hand, so-called '_in situ_' methods aim to eliminate sample transport altogether by carrying out DNP and NMR at the same magnetic field. Disadvantages of DNP NMR in the liquid state are the lower efficiency of the Overhauser effect at higher fields and excessive heating of polar solvents such as water due to application of high-intensity microwaves. Nonetheless, _in situ_ methods promise sample recyclability and greater retention of polarization before NMR detection, which also leads to greater concentration sensitivity. Here we cover the main classes of protocols for _in situ_ DNP NMR. Of these, temperature-jump and rapid-melt DNP NMR work by achieving hyperpolarization in the frozen state, followed by detection in the melted state. Lastly, we discuss the experimental developments that have enabled direct _in situ_ Overhauser DNP in the liquid state, followed by NMR detection without any intervening steps.

2.1.   Temperature jump DNP NMR: One way of eliminating the transport step of _ex situ_ techniques is by conducting DNP and NMR in the same magnet. DNP is conducted at low temperatures, after which the sample is rapidly melted _in situ_ for NMR spectroscopy. The first example of such an implementation was by Akasaka _et al._, who achieved the temperature jump using gas flowed through valves placed adjacent to the NMR probe.[129] In the _in situ_ DNP NMR apparatus implemented by the Griffin lab, the temperature jump is effected using an infrared pulse.[130,131] To overcome the lower Overhauser enhancements at higher fields, Griffin _et al._ use cross-polarization pulse sequences to transfer polarization from ^{1}H to low-γ nuclei such as ^{13}C or ^{15}N.[130] They have also reported direct detection of ^{13}C using total correlated spectroscopy (TOCSY).[131] In these experiments, the sample is cooled to 90 K or 100 K, hyperpolarized, melted rapidly using a CO_2 laser, and then subjected to NMR experiments. 10 μL of the sample is placed in a 2.5 mm o.d. quartz tube and the laser beam directed to the sample using an optical fiber. A gyrotron provides high-intensity continuous microwave irradiation required for DNP. The Kockenberger group have reported an improvement to this setup by conducting DNP at liquid-helium temperatures and using a high-power erbium-doped yttrium aluminium garnet (Er: YAG) laser for rapid melting of the sample.[132] Recently, Yoon _et al._ have reported the use of a frequency-tunable and power-tunable gyrotron that can be used for both DNP and melting steps. DNP is carried out using a microwave power of 1 W to 5 W, following which a high-power (> 50 W) microwave pulse is applied to melt the sample in < 1 s.[133] The sample is placed in a saddle coil for application of radiowaves, while microwaves are applied without the use of a resonator.

2.2. Rapid-melt DNP NMR: van Bentum's group have developed an *in situ* apparatus that works for mass-limited samples (10 nL to 1 μL), in which the sample is contained in a microfluidic capillary.[101] The capillary is placed on a microstrip probe that provides radiofrequency (RF) excitation for NMR spectroscopy. The capillary and microstrip are placed in a microwave cavity that can work in either resonant or non-resonant mode. Similar to the temperature-jump apparatus by Akasaka *et al.*,[129] this apparatus also uses gas flow to control the sample temperature. In van Bentum *et al.*'s apparatus, channels for liquid nitrogen and warm nitrogen gas (equally applicable to liquid helium) are fabricated in a poly(methyl methacrylate) (PMMA) block molded around the microwave cavity to enable rapid freezing and melting of the sample as it is moved over a distance of < 5 cm in this region of highest magnetic field homogeneity. Three separate regions are delineated within this range: a 77 K region for DNP, a 350 K region for melting and a 300 K region for NMR spectroscopy. An actuator moves the capillary between these regions, whose temperature is controlled by the flow of liquid nitrogen. DNP and NMR are carried out at the same magnetic field, making this an *in situ* detection protocol. DNP is carried out in the frozen solid state while NMR detection can be carried out either in the liquid state or in the frozen state. The small volume and ability for rapid melting/freezing eliminate the time required for sample preparation and repeatability of the melt-freeze cycle enables averaging over multiple scans. van Meerten *et al.* have demonstrated the implementation of this apparatus for high-frequency, multinuclear NMR experiments.[134]

2.3. In situ Overhauser DNP: While the above-mentioned *in situ* schemes provide improvements for spectroscopic measurements of small molecules, direct Overhauser enhancement would extend the benefits of hyperpolarization to larger molecules and biomacromolecular systems. The Prisner group and the Bennati group showed that direct Overhauser DNP enhancements for liquids at high magnetic fields can be larger than expected due to contributions from scalar HFI, provided the microwave power is high enough to approach saturation of the ESR transition for the paramagnetic matrix.[135–138] Double-resonant structures can be used to concentrate and enhance the microwave and RF magnetic fields at the sample, allowing the use of low-power microwave sources. To further increase the microwave power at the sample, Denysenkov *et al.* use both a resonator and a gyrotron in their high-field DNP spectrometer for liquids.[139] The increased microwave power provided them a three-fold gain in DNP enhancement. The size of resonant structures for microwaves is inherently restricted due to their smaller wavelengths (< 1 cm at frequencies > 35 GHz), which in turn restricts sample size. To allow larger samples, Dubroca *et al.* have implemented a quasi-optical system that directs gyrotron-sourced high-power microwaves directly to the sample contained in a non-resonant structure.[140]

Section IV: Instrumental challenges and outlook for liquid-state DNP NMR.

In this section, we speculate on future directions of method development for liquid-state DNP NMR. Since modern NMR is predominantly conducted at high fields to achieve better resolution and sensitivity, progress in instrumentation development for DNP NMR has also focused on enabling high-field operation in both *ex situ* and *in situ* methodologies. As mentioned previously, rather large DNP enhancements can be achieved at high fields if the EPR transition can be fully saturated. Therefore, it is desirable to enhance

microwave intensity at the sample volume. *In situ* and *ex situ* techniques have separate and characteristic challenges. We will discuss sample containment and flow setups in applications requiring larger or smaller volumes than those presently available in DNP NMR probes, development of PA, improvements in hardware, and the development of lab-on-a-chip DNP NMR setups for volume-limited samples. Finally, we mention advances in the field of low-field DNP NMR, which may be particularly impactful for field applications and *in vivo* imaging.

Challenges for *in situ* DNP NMR at high fields: *In situ* DNP NMR, particularly when DNP and NMR are conducted under identical physical conditions (field and temperature) is advantageous because it eliminates the problem of loss of polarization during the time taken to go from hyperpolarization conditions to NMR-spectroscopy conditions. However, the only mechanistic pathway for direct liquid-state DNP NMR is through the Overhauser effect, which becomes less efficient at higher fields, because the frequencies corresponding to the ZQ and DQ transitions become much greater than the modulation frequency of the HFI (provided by molecular motions). From a practical standpoint, *in situ* Overhauser DNP with direct NMR detection at the same field is also hindered by the high temperatures required to achieve the necessary correlation times for Overhauser enhancement. (As explained in Section III, point 1.2, supercritical DNP is a promising avenue for solving this problem in the case of small-molecule analytes.) Absorption of microwaves by polar solvents such as water can cause further heating, especially at higher frequencies. Lastly, Overhauser enhancement factors can be low for larger molecules due to their longer correlation times. Nonetheless, several recent reports demonstrate that it is possible to achieve enhancements in the range of 10 to 10^4 in liquid-state *in situ* DNP NMR at high frequencies. In these demonstrations, the high microwave power required to achieve near-saturation conditions is either generated directly by a gyrotron source,[135,122,124,140] or enhanced at the sample volume using microwave resonant structures (combined with RF resonant structures).[138]

Optimizing sample volume (resonant vs. non-resonant structures for microwave excitation): To achieve appreciable DNP enhancements in liquids, high microwave power is critical in order to saturate the EPR transition. Typically, resonant or non-resonant metallic structures, including coils, cylinders, and cylindrical/rectangular cavities, are used to couple the input microwaves or radiowaves to the sample. Resonators can be used to amplify microwave intensity at the sample when the use of high-power sources such as gyrotrons is expensive or inconvenient. For example, the Prisner group has reported cylinders made of flat metal helices, which are resonant for both EPR (up to 260 GHz) and NMR frequencies.[135,136,139] The Bennati group use cylindrical TE011 cavities to obtain EPR saturation at 94 GHz, while electron nuclear double resonance (ENDOR) coils are used to localize radiowaves over the sample volume.[137,138] However, the dimensions of resonators become smaller as frequency increases (wavelength decreases), resulting in limits on the sample volume (< 1 μL). This problem is exacerbated in double-resonant structures, where the wavelength mismatch of microwaves and radiowaves leads to a situation where only a small fraction of the available sample volume in the RF resonator can be filled because the upper limit of sample volume is determined by the microwave

resonator. A solution to this problem is to miniaturize the RF resonator so its size is comparable to the EPR resonator.[141] However, this still results in sub-microliter sample volumes. Additionally, due to their higher Q-factors, microwave resonant structures have inherently low bandwidths, which deteriorates the sensitivity by allowing DNP enhancement from only a small fraction of the available EPR spectrum. Thus, the use of resonators proves advantageous for mass-limited samples but is less so when the sample quantity is not a limiting factor. Non-resonant structures may be used to localize incident microwaves at the sample volume. These are not size-restricted and can therefore accommodate larger sample volumes. However, these necessitate the use of high-power microwave sources to saturate the EPR transition. Ultimately, structures for localizing microwaves and radiowaves must be chosen to maximize SNR by optimizing sample volume, B_1 intensity, and fraction of the EPR spectrum excited. Additionally, resonators must be designed to separate the regions of electric and magnetic field so that sample heating of high-loss dielectric samples, such as aqueous solutions, is minimized.

Large-volume structures are desirable when sample quantity is not limited, so that a large amount of sample may be used to achieve the best possible SNR. On the other hand, many samples are inherently mass-limited as well as concentration-limited, e.g., membrane proteins and other biomacromolecular samples prone to aggregation. Liquid-state DNP NMR of such samples can potentially provide information about dynamics of structure, conformation, and solvation, which is not obtainable through solid-state MAS DNP NMR for all protein samples. Resonators are more suited to such mass-limited and concentration-limited samples. To maximize the SNR in this case, the sample volume should be comparable to the volume of the resonator. Novel approaches are being applied to solve the above-mentioned challenges in resonator design. In Fabry-Perot resonators, the resonator dimension must be limited in only one direction. This allows the sample volume to be extended in the remaining two directions, resulting in large-volume planar structures with sample volumes of tens of microliters.[142–144] The Smirnov group has developed double-resonant structures in which photonic bandgap microwave resonators are incorporated with NMR coils. These structures are also size-limited in only one dimension, resulting in sample volumes of several microliters.[145]

***Ex situ* DNP NMR at high fields:** It is generally accepted that in the case of d-DNP, increasing the field at which DNP is conducted increases the maximum enhancement but also increases the time required to reach this maximum. Further, no appreciable sensitivity gains are obtained after a field of about 7 T. Therefore, further improvements to *ex situ* DNP NMR are likely to focus on first, decreasing loss of polarization between the DNP and NMR steps and second, increasing the amount of hyperpolarized material to offset the expense of time and cryogen while building up hyperpolarization (the second point is particularly important for clinical applications, in which the amount of sample is not a limiting factor).

• High throughput: Increasing the throughput of the hyperpolarization stage is desirable because: first, it overcomes the time lost during buildup of hyperpolarization, which is a limiting step in d-DNP; and second, it partially overcomes the lack of sample recyclability. Ardenkjær-Larsen *et al.* have reported a d-DNP polarizer that can simultaneously produce

up to three hyperpolarized samples of up to 2 g with a buildup time of 20 min.[146] Further, their system uses a closed loop to recycle the cryogen required to cool the sample down for hyperpolarization, easing the massive cryogen requirements of d-DNP. Another similar design of d-DNP spectrometer reported recently can accommodate two samples, and can be modified to accomodate up to four samples.[147] Bornet *et al.* have shown that cross-polarization from ^{1}H to ^{13}C during the hyperpolarization step can be preserved through dissolution, dramatically increasing the DNP throughput for low-gamma nuclei.[148]

• Preserving hyperpolarization: Developing hardware for efficient transport of hyperpolarized sample is an active area in DNP research, since *ex situ* schemes such as d-DNP are still limited by the problems of sample depolarization during transport and sample dilution in the dissolution step. Kou il *et al.* have reported a new transportation protocol in which the sample is hyperpolarized and transferred to the site of NMR in the solid form ("bullet DNP") in 70 ms.[115] Dissolution is carried out just before NMR, and the amount of solvent can be adjusted as required for NMR spectroscopy. This makes the method scalable to small volumes.

Polarizing agents: Exogenous radicals such as TOTAPOL,[149] AMUPOL,[150] BDPA and its derivatives, and trityl are typically used as PAs in DNP NMR. Recent years have seen the development of biradicals, which contain two rigidly linked paramagnetic moieties, that provide improved DNP enhancements, particularly via the cross effect.[151,152] For applicability at high fields, Lund *et al.* have recently developed 'TinyPols', which are water-soluble biradicals with strong dipolar coupling between the two unpaired electrons.[153] In d-DNP, Gd^{3+}-doping has been shown to have a strong influence on polarization enhancement of ^{13}C compounds such as pyruvate.[154–156] Below we summarize the most recent developments in PAs, based on different methodologies of solution DNP NMR.

• PA for scalar Overhauser effect: Earlier reports of direct Overhauser enhancement involved predominantly dipolar HFI of protons, resulting in the conventional thought that enhancements become small as field is increased. While this may be true for hyperpolarization of high-γ nuclei such as protons, the Bennati group has recently shown that enhancement factors of the order of 1000 can be obtained for ^{13}C in Overhauser DNP for fields in the range of 1 T to 10 T.[138] These enhancements have been explained as arising from the scalar HFI between the ^{13}C-containing molecule and paramagnetic radical, and the key features of the mechanism have been identified.[157] Further elucidation of the mechanistic origins of these large ^{13}C enhancements is likely to result in new PA for direct Overhauser enhancement in the solution state.[158,159]

• PA for *ex situ* techniques: In *ex situ* techniques where hyperpolarization and NMR/MRI are separated by a transport step, the paramagnetic matrix is required for DNP but becomes undesirable in the transport and NMR steps because it causes loss of polarization and broadening of NMR lines. The PA may be separated from the sample by physical methods, e.g., filterable agents[160,161] or immobilization on a solid substrate.[162,120,121,163] An elegant means to generate longer-lasting, transportable hyperpolarized samples is photo-generation of radicals that re-combine when the temperature is increased after the hyperpolarization

step.[164,165] This provides a way to eliminate the undesirable paramagnetic matrix after the hyperpolarization step.

• Triplet DNP for liquid samples: Photo-induced triplet states can be used to generate hyperpolarization that is independent of temperature and magnetic field strength.[166] Kagawa *et al.* have recently reported protocols for preparing a wide range of hyperpolarized samples at room temperature using the photo-induced triplet state of pentacene,[167] and have further used triplet DNP in conjunction with the d-DNP protocol to obtain hyperpolarized solutions at both low and high fields.[168,169] The Yanai group is active in developing PAs with favorable properties such as improved air stability[170] and water-solubility.[171] The Bennati group has reported liquid-state triplet DNP using photoexcitable fullerene-nitroxide derivatives.[172]

Mass-limited samples: Some examples of applications for mass-limited and concentration-limited liquid-state samples that particularly benefit from hyperpolarization include: identification of natural products, metabolites of pharmaceuticals and agrochemicals, and characterization of compounds from combinatorial chemistry;[173,174] studies of structure and dynamics of membrane proteins and other biomacromolecules that are difficult to isolate and prone to aggregation at the high concentration typically needed for standard NMR measurements;[175] and in-cell NMR.[176,177] Such applications require the ability to sense both small volumes and small concentrations. Double-resonant structures provide sample volumes of nanoliters but the fill factor for the RF part of the double-resonator is very small, resulting in poor sensitivity. (For comparison, CapNMR finds widespread use in solution NMR but requires microliter volumes.[178]) Planar microcoils are easier to fabricate down to nL volumes, and find applications in on-chip NMR devices.[179] Recently, Solmaz *et al.* have demonstrated a silicon-chip-based device for DNP NMR of aqueous solutions of TEMPO radical at room temperature.[180] A sample volume of about 1 nL is contained in a capillary that is placed over the double NMR/ESR microcoils.

Low-field DNP NMR: Although recent developments in DNP NMR have focused on extending applicability to high-field NMR, low-field NMR is also an emerging area that stands to benefit from sensitivity enhancements provided by DNP. Developments in low-field DNP NMR seek to increase resolution while maximizing hyperpolarization. Maly *et al.* have shown recently that is possible to improve both sensitivity and resolution even at low fields by improving field homogeneity.[181] The ability to conduct DNP NMR at low fields is also desirable for portable setups.[97]

Conclusion: In this review, we have attempted to provide an overview of the conceptual basis, applications, and instrumentation for a wide range of schemes for liquid-state CW DNP NMR. Liquid-state DNP has broad potential applications, particularly in the areas of metabolite characterization, imaging, characterization of transient species in reaction mechanisms, and studies of structure, conformation, and solvation dynamics for precious biomolecular samples. Approaches to liquid-state DNP NMR must take into account the sample type, size, and application. Some applications involve samples that are inherently limited in quantity and/or concentration (metabolomics, transient species, some

biomacromolecular samples). On the other hand, in applications like imaging, it is desirable to have high throughputs of hyperpolarized sample, and amount of sample is not a limiting factor. In *in vivo* imaging, the hyperpolarized sample is injected into a specimen and thus, there is a natural separation of locations for hyperpolarization and NMR. Such applications necessitate the use of *ex situ* DNP methodologies such as dissolution DNP. Direct DNP in liquids is of interest for biomacromolecular systems that are difficult to express, purify, and reconstitute, and that may become denatured and/or aggregate through rapid changes in physical conditions. While brute-force methods may sometimes offer greater effective sensitivity at high fields, DNP promises sensitivity gains at low and intermediate frequencies. In general, all DNP methodologies would benefit from high-field operability to take advantage of the high resolution and sensitivity provided by modern high-field NMR spectrometers. On the other hand, there is interest in improving the resolution of low-field DNP since larger enhancements can be obtained at low fields and, additionally, because low fields are favorable for applications such as *in vivo* imaging and compact spectrometers. PA for which the scalar HFI is dominant are likely to facilitate greater DNP enhancements at high fields. Another way to obtain field-independent DNP enhancement is using photo-excited triplets to saturate the electronic spin system. Supercritical DNP may also be impactful for high-field NMR of small-molecule analytes by faster relaxation frequencies, and by providing a proton-free solvent that is not prone to dielectric heating. Most detection schemes for DNP NMR employ high-power microwave sources such as gyrotrons to saturate the EPR transition. On the other hand, double-resonant structures eliminate the need for using high-power microwave sources but require advances in miniaturization to confine radiowaves and microwaves in similar volumes. The varied methodologies of *ex situ* and *in situ* liquid DNP provide a large playing field with multi-faceted opportunities for advancement, with the ultimate promise of revealing hitherto unavailable information about dynamic processes occurring in liquids.

Acknowledgments

Biographies

Veronika Szalai joined the National Institute of Standards & Technology (NIST) in 2010 and is currently a Project Leader in the Biophysical and Biomedical Measurement Group. She received an A.B. in Chemistry from Bryn Mawr College and a Ph.D. in Inorganic Chemistry from Yale University. After completing post-doctoral work at the University of North Carolina at Chapel Hill, Veronika advanced to the rank of associate professor (with tenure) in the Department of Chemistry & Biochemistry at the University of Maryland Baltimore

County. Her laboratory at NIST focuses on advanced electron paramagnetic resonance (EPR) spectroscopy and instrumentation development for measurements of biological and nanomaterial systems and, previously, on tools for *in operando* reactivity measurements of nanomaterials.

Nandita Abhyankar is a Visiting Fellow working jointly at the Institute for Research in Applied Physics and Electronics (IREAP) at UMD, College Park and the Physical Measurement Laboratory (PML) at NIST. Here she works on designing, fabricating, and implementing microresonators for electron paramagnetic resonance (EPR) spectroscopy. She obtained an M.S. in Chemistry from Pune University in India and her Ph.D. in Physical Chemistry from Florida State University, where she worked on methods for synthesizing metal-organic frameworks (MOFs) and studying their electric and magnetic properties.

References:

(1). Barnes AB; De Paëpe G; van der Wel PCA; Hu K-N; Joo C-G; Bajaj VS; Mak-Jurkauskas ML; Sirigiri JR; Herzfeld J; Temkin RJ; Griffin RG High-Field Dynamic Nuclear Polarization for Solid and Solution Biological NMR. Appl. Magn. Reson. 2008, 34 (3–4), 237–263. 10.1007/s00723-008-0129-1. [PubMed: 19194532]

(2). Lacabanne D; Fogeron M-L; Wiegand T; Cadalbert R; Meier BH; Böckmann A Protein Sample Preparation for Solid-State NMR Investigations. Prog. Nucl. Magn. Reson. Spectrosc. 2019, 110, 20–33. 10.1016/j.pnmrs.2019.01.001. [PubMed: 30803692]

(3). Maly T; Debelouchina GT; Bajaj VS; Hu K-N; Joo C-G; Mak–Jurkauskas ML; Sirigiri JR; van der Wel PCA; Herzfeld J; Temkin RJ; Griffin RG Dynamic Nuclear Polarization at High Magnetic Fields. J. Chem. Phys. 2008, 128 (5), 052211. 10.1063/1.2833582. [PubMed: 18266416]

(4). Corzilius B High-Field Dynamic Nuclear Polarization. Annu. Rev. Phys. Chem. 2020, 71 (1), 143–170. 10.1146/annurev-physchem-071119-040222. [PubMed: 32074473]

(5). Can TV; Ni QZ; Griffin RG Mechanisms of Dynamic Nuclear Polarization in Insulating Solids. Spec. Issue Recent Achiev. New Dir. Biomol. Solid State NMR 2015, 253, 23–35. 10.1016/j.jmr.2015.02.005.

(6). Bennati M; Tkach I; Türke M-T Dynamic Nuclear Polarization in Liquids. In Electron Paramagnetic Resonance; Gilbert BC, Murphy DM, Chechik V, Eds.; Royal Society of Chemistry: Cambridge, 2010; Vol. 22, pp 155–182. 10.1039/9781849730877-00155.

(7). Ravera E; Luchinat C; Parigi G Basic Facts and Perspectives of Overhauser DNP NMR. J. Magn. Reson. 2016, 264, 78–87. 10.1016/j.jmr.2015.12.013. [PubMed: 26920833]

(8). van Bentum J; van Meerten B; Sharma M; Kentgens A Perspectives on DNP-Enhanced NMR Spectroscopy in Solutions. J. Magn. Reson. 2016, 264, 59–67. 10.1016/j.jmr.2016.01.010. [PubMed: 26920831]

(9). Hausser KH; Stehlik D Dynamic Nuclear Polarization in Liquids. In Advances in Magnetic and Optical Resonance; Elsevier, 1968; Vol. 3, pp 79–139. 10.1016/B978-1-4832-3116-7.50010-2.

(10). Overhauser AW Polarization of Nuclei in Metals. Phys. Rev. 1953, 92 (2), 411–415. 10.1103/PhysRev.92.411.

(11). Abragam A; Goldman M Principles of Dynamic Nuclear Polarisation. Rep. Prog. Phys. 1978, 41 (3), 395–467. 10.1088/0034-4885/41/3/002.

(12). Carver TR; Slichter CP Polarization of Nuclear Spins in Metals. Phys. Rev. 1953, 92 (1), 212–213. 10.1103/PhysRev.92.212.2.

(13). Abragam A Overhauser Effect in Nonmetals. Phys. Rev. 1955, 98 (6), 1729–1735. 10.1103/PhysRev.98.1729.

(14). Solomon I Relaxation Processes in a System of Two Spins. Phys. Rev. 1955, 99 (2), 559–565. 10.1103/PhysRev.99.559.

(15). Ardenkjaer-Larsen JH; Fridlund B; Gram A; Hansson G; Hansson L; Lerche MH; Servin R; Thaning M; Golman K Increase in Signal-to-Noise Ratio of > 10,000 Times in Liquid-State NMR. Proc. Natl. Acad. Sci. 2003, 100 (18), 10158–10163. 10.1073/pnas.1733835100. [PubMed: 12930897]

(16). Wang X; Isley III WC; Salido SI; Sun Z; Song L; Tsai KH; Cramer CJ; Dorn HC Optimization and Prediction of the Electron–Nuclear Dipolar and Scalar Interaction in 1H and 13C Liquid State Dynamic Nuclear Polarization. Chem. Sci. 2015, 6 (11), 6482–6495. 10.1039/C5SC02499D. [PubMed: 30090267]

(17). Gizatullin B; Gafurov M; Vakhin A; Rodionov A; Mamin G; Orlinskii S; Mattea C; Stapf S Native Vanadyl Complexes in Crude Oil as Polarizing Agents for In Situ Proton Dynamic Nuclear Polarization. Energy Fuels 2019, 33 (11), 10923–10932. 10.1021/acs.energyfuels.9b03049.

(18). Hwang CF; Hill DA New Effect in Dynamic Polarization. Phys. Rev. Lett. 1967, 18 (4), 110–112. 10.1103/PhysRevLett.18.110.

(19). Hwang CF; Hill DA Phenomenological Model for the New Effect in Dynamic Polarization. Phys. Rev. Lett. 1967, 19 (18), 1011–1014. 10.1103/PhysRevLett.19.1011.

(20). Borghini M Spin-Temperature Model of Nuclear Dynamic Polarization Using Free Radicals. Phys. Rev. Lett. 1968, 20 (9), 419–421. 10.1103/PhysRevLett.20.419.

(21). Wenckebach W Th. Dynamic Nuclear Polarization via Thermal Mixing: Beyond the High Temperature Approximation. J. Magn. Reson. 2017, 277, 68–78. 10.1016/j.jmr.2017.01.020. [PubMed: 28237893]

(22). Equbal A; Leavesley A; Jain SK; Han S Cross-Effect Dynamic Nuclear Polarization Explained: Polarization, Depolarization, and Oversaturation. J. Phys. Chem. Lett. 2019, 10 (3), 548–558. 10.1021/acs.jpclett.8b02834. [PubMed: 30645130]

(23). Grazia Concilio M; Soundararajan M; Frydman L; Kuprov I High-Field Solution State DNP Using Cross-Correlations. J. Magn. Reson. 2021, 106940. 10.1016/j.jmr.2021.106940. [PubMed: 33865207]

(24). Kundu K; Feintuch A; Vega S Theoretical Aspects of the Cross Effect Enhancement of Nuclear Polarization under Static Dynamic Nuclear Polarization Conditions. J. Phys. Chem. Lett. 2019, 10 (8), 1769–1778. 10.1021/acs.jpclett.8b03615. [PubMed: 30864810]

(25). Equbal A; Li Y; Tabassum T; Han S Crossover from a Solid Effect to Thermal Mixing 1H Dynamic Nuclear Polarization with Trityl-OX063. J. Phys. Chem. Lett. 2020, 11 (9), 3718–3723. 10.1021/acs.jpclett.0c00830. [PubMed: 32315195]

(26). Wangsness RK; Bloch F The Dynamical Theory of Nuclear Induction. Phys. Rev. 1953, 89 (4), 728–739. 10.1103/PhysRev.89.728.

(27). Redfield AG On the Theory of Relaxation Processes. IBM J. Res. Dev. 1957, 1 (1), 19–31. 10.1147/rd.11.0019.

(28). Karabanov A; Kwiatkowski G; Perotto CU; Wiśniewski D; McMaster J; Lesanovsky I; Köckenberger W Dynamic Nuclear Polarisation by Thermal Mixing: Quantum Theory and Macroscopic Simulations. Phys. Chem. Chem. Phys. 2016, 18 (43), 30093–30104. 10.1039/C6CP04345C. [PubMed: 27775111]

(29). Kundu K; Feintuch A; Vega S Theoretical Aspects of the Cross Effect Enhancement of Nuclear Polarization under Static Dynamic Nuclear Polarization Conditions. J. Phys. Chem. Lett. 2019, 10 (8), 1769–1778. 10.1021/acs.jpclett.8b03615. [PubMed: 30864810]

(30). Equbal A; Li Y; Tabassum T; Han S Crossover from a Solid Effect to Thermal Mixing 1H Dynamic Nuclear Polarization with Trityl-OX063. J. Phys. Chem. Lett. 2020, 11 (9), 3718–3723. 10.1021/acs.jpclett.0c00830. [PubMed: 32315195]

(31). Corzilius B Theory of Solid Effect and Cross Effect Dynamic Nuclear Polarization with Half-Integer High-Spin Metal Polarizing Agents in Rotating Solids. Phys. Chem. Chem. Phys. 2016, 18 (39), 27190–27204. 10.1039/C6CP04621E. [PubMed: 27548726]

(32). Lumata L; Jindal AK; Merritt ME; Malloy CR; Sherry AD; Kovacs Z DNP by Thermal Mixing under Optimized Conditions Yields > 60 000-Fold Enhancement of 89Y NMR Signal. J. Am. Chem. Soc. 2011, 133 (22), 8673–8680. 10.1021/ja201880y. [PubMed: 21539398]

(33). Giraudeau P Challenges and Perspectives in Quantitative NMR: Challenges and Perspectives in Quantitative NMR. Magn. Reson. Chem. 2017, 55 (1), 61–69. 10.1002/mrc.4475. [PubMed: 27370178]

(34). Franck JM; Han S Overhauser Dynamic Nuclear Polarization for the Study of Hydration Dynamics, Explained. In Methods in Enzymology; Elsevier, 2019; Vol. 615, pp 131–175. 10.1016/bs.mie.2018.09.024. [PubMed: 30638529]

(35). Armstrong BD; Choi J; López C; Wesener DA; Hubbell W; Cavagnero S; Han S Site-Specific Hydration Dynamics in the Nonpolar Core of a Molten Globule by Dynamic Nuclear Polarization of Water. J. Am. Chem. Soc. 2011, 133 (15), 5987–5995. 10.1021/ja111515s. [PubMed: 21443207]

(36). McCarney ER; Armstrong BD; Kausik R; Han S Dynamic Nuclear Polarization Enhanced Nuclear Magnetic Resonance and Electron Spin Resonance Studies of Hydration and Local Water Dynamics in Micelle and Vesicle Assemblies. Langmuir 2008, 24 (18), 10062–10072. 10.1021/la800334k. [PubMed: 18700788]

(37). Armstrong BD; Han S Overhauser Dynamic Nuclear Polarization to Study Local Water Dynamics. J. Am. Chem. Soc. 2009, 131 (13), 4641–4647. 10.1021/ja809259q. [PubMed: 19290661]

(38). Segawa TF; Doppelbauer M; Garbuio L; Doll A; Polyhach YO; Jeschke G Water Accessibility in a Membrane-Inserting Peptide Comparing Overhauser DNP and Pulse EPR Methods. J. Chem. Phys. 2016, 144 (19), 194201. 10.1063/1.4948988. [PubMed: 27208942]

(39). Chaubey B; Dey A; Banerjee A; Chandrakumar N; Pal S Assessment of the Role of 2,2,2-Trifluoroethanol Solvent Dynamics in Inducing Conformational Transitions in Melittin: An Approach with Solvent 19F Low-Field NMR Relaxation and Overhauser Dynamic Nuclear Polarization Studies. J. Phys. Chem. B 2020, 124 (28), 5993–6003. 10.1021/acs.jpcb.0c03544. [PubMed: 32573229]

(40). Kim J; Liu M; Hilty C Modeling of Polarization Transfer Kinetics in Protein Hydration Using Hyperpolarized Water. J. Phys. Chem. B 2017, 121 (27), 6492–6498. 10.1021/acs.jpcb.7b03052. [PubMed: 28613875]

(41). Kade ávek P; Ferrage F; Bodenhausen G; Kurzbach D High-Resolution NMR of Folded Proteins in Hyperpolarized Physiological Solvents. Chem. - Eur. J. 2018, 24 (51), 13418–13423. 10.1002/chem.201802885. [PubMed: 29969165]

(42). Chappuis Q; Milani J; Vuichoud B; Bornet A; Gossert AD; Bodenhausen G; Jannin S Hyperpolarized Water to Study Protein–Ligand Interactions. J. Phys. Chem. Lett. 2015, 6 (9), 1674–1678. 10.1021/acs.jpclett.5b00403. [PubMed: 26263332]

(43). Kim J; Mandal R; Hilty C Observation of Fast Two-Dimensional NMR Spectra during Protein Folding Using Polarization Transfer from Hyperpolarized Water. J. Phys. Chem. Lett. 2019, 10 (18), 5463–5467. 10.1021/acs.jpclett.9b02197. [PubMed: 31442055]

(44). Akbey Ü; Oschkinat H Structural Biology Applications of Solid State MAS DNP NMR. J. Magn. Reson. 2016, 269, 213–224. 10.1016/j.jmr.2016.04.003. [PubMed: 27095695]

(45). Jaudzems K; Polenova T; Pintacuda G; Oschkinat H; Lesage A DNP NMR of Biomolecular Assemblies. J. Struct. Biol. 2019, 206 (1), 90–98. 10.1016/j.jsb.2018.09.011. [PubMed: 30273657]

(46). Kim J; Mandal R; Hilty C Characterization of Membrane Protein-Lipid Interactions in Unfolded OmpX with Enhanced Time Resolution by Hyperpolarized NMR. ChemBioChem 2020, cbic.202000271. 10.1002/cbic.202000271.

(47). Szekely O; Olsen GL; Felli IC; Frydman L High-Resolution 2D NMR of Disordered Proteins Enhanced by Hyperpolarized Water. Anal. Chem. 2018, 90 (10), 6169–6177. 10.1021/acs.analchem.8b00585. [PubMed: 29528228]

(48). Wang Y; Kim J; Hilty C Determination of Protein–Ligand Binding Modes Using Fast Multi-Dimensional NMR with Hyperpolarization. Chem. Sci. 2020, 11 (23), 5935–5943. 10.1039/D0SC00266F. [PubMed: 32874513]

(49). Wang Y; Ragavan M; Hilty C Site Specific Polarization Transfer from a Hyperpolarized Ligand of Dihydrofolate Reductase. J. Biomol. NMR 2016, 65 (1), 41–48. 10.1007/s10858-016-0037-x. [PubMed: 27189223]

(50). Lee Y; Zeng H; Mazur A; Wegstroth M; Carlomagno T; Reese M; Lee D; Becker S; Griesinger C; Hilty C Hyperpolarized Binding Pocket Nuclear Overhauser Effect for Determination of Competitive Ligand Binding. Angew. Chem. Int. Ed. 2012, 51 (21), 5179–5182. 10.1002/anie.201201003.

(51). Min H; Sekar G; Hilty C Polarization Transfer from Ligands Hyperpolarized by Dissolution Dynamic Nuclear Polarization for Screening in Drug Discovery. ChemMedChem 2015, 10 (9), 1559–1563. 10.1002/cmdc.201500241. [PubMed: 26315550]

(52). Brogi S; Ramalho TC; Kuca K; Medina-Franco JL; Valko M Editorial: In Silico Methods for Drug Design and Discovery. Front. Chem. 2020, 8, 612. 10.3389/fchem.2020.00612. [PubMed: 32850641]

(53). Bowen S; Hilty C Time-Resolved Dynamic Nuclear Polarization Enhanced NMR Spectroscopy. Angew. Chem. Int. Ed. 2008, 47 (28), 5235–5237. 10.1002/anie.200801492.

(54). Bowen S; Hilty C Temporal Chemical Shift Correlations in Reactions Studied by Hyperpolarized Nuclear Magnetic Resonance. Anal. Chem. 2009, 81 (11), 4543–4547. 10.1021/ac900456q. [PubMed: 19388628]

(55). Zhang G; Schilling F; Glaser SJ; Hilty C Reaction Monitoring Using Hyperpolarized NMR with Scaling of Heteronuclear Couplings by Optimal Tracking. J. Magn. Reson. 2016, 272, 123–128. 10.1016/j.jmr.2016.09.006. [PubMed: 27689531]

(56). Jensen PR; Meier S Catalytic Cycle of Carbohydrate Dehydration by Lewis Acids: Structures and Rates from Synergism of Conventional and DNP NMR. Chem. Commun. 2020, 56 (46), 6245–6248. 10.1039/D0CC01756F.

(57). Jensen PR; Meier S; Ardenkjær-Larsen JH; Duus JØ; Karlsson M; Lerche MH Detection of Low-Populated Reaction Intermediates with Hyperpolarized NMR. Chem. Commun. 2009, No. 34, 5168. 10.1039/b910626j.

(58). Boeg PA; Duus JØ; Ardenkjær-Larsen JH; Karlsson M; Mossin S Real-Time Detection of Intermediates in Rhodium-Catalyzed Hydrogenation of Alkynes and Alkenes by Dissolution DNP. J. Phys. Chem. C 2019, 123 (15), 9949–9956. 10.1021/acs.jpcc.9b01376.

(59). Chen C-H; Shih W-C; Hilty C In Situ Determination of Tacticity, Deactivation, and Kinetics in [Rac-(C2H4(1-Indenyl)2)ZrMe][B(C6F5)4] and [Cp2ZrMe][B(C6F5)4]-Catalyzed Polymerization of 1-Hexene Using 13C Hyperpolarized NMR. J. Am. Chem. Soc. 2015, 137 (21), 6965–6971. 10.1021/jacs.5b04479. [PubMed: 25961793]

(60). Lee Y; Heo GS; Zeng H; Wooley KL; Hilty C Detection of Living Anionic Species in Polymerization Reactions Using Hyperpolarized NMR. J. Am. Chem. Soc. 2013, 135 (12), 4636–4639. 10.1021/ja4001008. [PubMed: 23461287]

(61). Weber EMM; Kress T; Abergel D; Sewsurn S; Azaïs T; Kurzbach D Assessing the Onset of Calcium Phosphate Nucleation by Hyperpolarized Real-Time NMR. Anal. Chem. 2020, 92 (11), 7666–7673. 10.1021/acs.analchem.0c00516. [PubMed: 32378878]

(62). Lerche MH; Meier S; Jensen PR; Baumann H; Petersen BO; Karlsson M; Duus JØ; Ardenkjær-Larsen JH Study of Molecular Interactions with 13C DNP-NMR. J. Magn. Reson. 2010, 203 (1), 52–56. 10.1016/j.jmr.2009.11.020. [PubMed: 20022775]

(63). Liu M; Zhang G; Mahanta N; Lee Y; Hilty C Measurement of Kinetics and Active Site Distances in Metalloenzymes Using Paramagnetic NMR with 13C Hyperpolarization. J. Phys. Chem. Lett. 2018, 9 (9), 2218–2221. 10.1021/acs.jpclett.8b00350. [PubMed: 29624056]

(64). Shishmarev D; Wright AJ; Rodrigues TB; Pileio G; Stevanato G; Brindle KM; Kuchel PW Sub-Minute Kinetics of Human Red Cell Fumarase: 1H Spin-Echo NMR Spectroscopy and 13C Rapid-Dissolution Dynamic Nuclear Polarization. NMR Biomed. 2018, 31 (3), e3870. 10.1002/nbm.3870.

(65). Drachman N; Kadlecek S; Duncan I; Rizi R Quantifying Reaction Kinetics of the Non-Enzymatic Decarboxylation of Pyruvate and Production of Peroxymonocarbonate with Hyperpolarized 13C-NMR. Phys. Chem. Chem. Phys. 2017, 19 (29), 19316–19325. 10.1039/C7CP02041D. [PubMed: 28703828]

(66). Timm KN; Hu D-E; Williams M; Wright AJ; Kettunen MI; Kennedy BWC; Larkin TJ; Dzien P; Marco-Rius I; Bohndiek SE; Brindle KM Assessing Oxidative Stress in Tumors by Measuring the Rate of Hyperpolarized [1– 13C]-Dehydroascorbic Acid Reduction Using 13C Magnetic Resonance Spectroscopy. J. Biol. Chem. 2017, 292 (5), 1737–1748. 10.1074/jbc.M116.761536. [PubMed: 27994059]

(67). Tickner Ben. J.; Rayner PJ; Duckett SB Using SABRE Hyperpolarized 13C NMR Spectroscopy to Interrogate Organic Transformations of Pyruvate. Anal. Chem. 2020, 92 (13), 9095–9103. 10.1021/acs.analchem.0c01334. [PubMed: 32510200]

(68). Bowen S; Sekar G; Hilty C Rapid Determination of Biosynthetic Pathways Using Fractional Isotope Enrichment and High-Resolution Dynamic Nuclear Polarization Enhanced NMR: BIOSYNTHETIC PATHWAYS STUDIED BY HYPERRPOLARIZED NMR. NMR Biomed. 2011, 24 (8), 1016–1022. 10.1002/nbm.1679. [PubMed: 21387448]

(69). Kjeldsen C; Ardenkjær-Larsen JH; Duus, Jens. Ø. Unexpected Anomeric Acceptor Preference Observed Using DDNP NMR for Transglycosylation Studies of β-Galactosidases. Biochemistry 2020, 59 (31), 2903–2908. 10.1021/acs.biochem.0c00390. [PubMed: 32686402]

(70). Golman K; in 't Zandt R; Thaning M Real-Time Metabolic Imaging. Proc. Natl. Acad. Sci. 2006, 103 (30), 11270–11275. 10.1073/pnas.0601319103. [PubMed: 16837573]

(71). Lerche MH; Meier S; Jensen PR; Hustvedt S-O; Karlsson M; Duus JØ; Ardenkjaer-Larsen JH Quantitative Dynamic Nuclear Polarization-NMR on Blood Plasma for Assays of Drug Metabolism. NMR Biomed. 2011, 24 (1), 96–103. 10.1002/nbm.1561. [PubMed: 20862657]

(72). Bohndiek SE; Kettunen MI; Hu D; Kennedy BWC; Boren J; Gallagher FA; Brindle KM Hyperpolarized [1– 13C]-Ascorbic and Dehydroascorbic Acid: Vitamin C as a Probe for Imaging Redox Status in Vivo. J. Am. Chem. Soc. 2011, 133 (30), 11795–11801. 10.1021/ja2045925. [PubMed: 21692446]

(73). Simmler C; Napolitano JG; McAlpine JB; Chen S-N; Pauli GF Universal Quantitative NMR Analysis of Complex Natural Samples. Curr. Opin. Biotechnol. 2014, 25, 51–59. 10.1016/j.copbio.2013.08.004. [PubMed: 24484881]

(74). Dzien P; Fages A; Jona G; Brindle KM; Schwaiger M; Frydman L Following Metabolism in Living Microorganisms by Hyperpolarized 1H NMR. J. Am. Chem. Soc. 2016, 138 (37), 12278–12286. 10.1021/jacs.6b07483. [PubMed: 27556338]

(75). Jensen PR; Karlsson M; Lerche MH; Meier S Real-Time DNP NMR Observations of Acetic Acid Uptake, Intracellular Acidification, and of Consequences for Glycolysis and Alcoholic Fermentation in Yeast. Chem. - Eur. J. 2013, 19 (40), 13288–13293. 10.1002/chem.201302429. [PubMed: 24019026]

(76). Lerche MH; Jensen PR; Karlsson M; Meier S NMR Insights into the Inner Workings of Living Cells. Anal. Chem. 2015, 87 (1), 119–132. 10.1021/ac501467x. [PubMed: 25084065]

(77). Kumar A; Kuhn L; Balbach J In-Cell NMR: Analysis of Protein–Small Molecule Interactions, Metabolic Processes, and Protein Phosphorylation. Int. J. Mol. Sci. 2019, 20 (2), 378. 10.3390/ijms20020378. [PubMed: 30658393]

(78). Warnet XL; Arnold AA; Marcotte I; Warschawski DE In-Cell Solid-State NMR: An Emerging Technique for the Study of Biological Membranes. Biophys. J. 2015, 109 (12), 2461–2466. 10.1016/j.bpj.2015.10.041. [PubMed: 26682804]

(79). Judge PT; Sesti EL; Price LE; Albert BJ; Alaniva N; Saliba EP; Halbritter T; Sigurdsson S. Th.; Kyei GB; Barnes AB Dynamic Nuclear Polarization with Electron Decoupling in Intact Human Cells and Cell Lysates. J. Phys. Chem. B 2020, 124 (12), 2323–2330. 10.1021/acs.jpcb.9b10494. [PubMed: 32083876]

(80). Zhelev Z; Bakalova R; Aoki I; Matsumoto K; Gadjeva V; Anzai K; Kanno I Nitroxyl Radicals for Labeling of Conventional Therapeutics and Noninvasive Magnetic Resonance Imaging of Their Permeability for Blood–Brain Barrier: Relationship between Structure, Blood Clearance, and MRI Signal Dynamic in the Brain. Mol. Pharm. 2009, 6 (2), 504–512. 10.1021/mp800175k. [PubMed: 19718801]

(81). Zhelev Z; Bakalova R; Aoki I; Matsumoto K; Gadjeva V; Anzai K; Kanno I Nitroxyl Radicals as Low Toxic Spin-Labels for Non-Invasive Magnetic Resonance Imaging of Blood–Brain Barrier Permeability for Conventional Therapeutics. Chem Commun 2009, No. 1, 53–55. 10.1039/B816878D.

(82). Kishimoto S; Oshima N; Krishna MC; Gillies RJ Direct and Indirect Assessment of Cancer Metabolism Explored by MRI. NMR Biomed. 2019, 32 (10). 10.1002/nbm.3966.

(83). Asavei T; Bobeica M; Nastasa V; Manda G; Naftanaila F; Bratu O; Mischianu D; Cernaianu MO; Ghenuche P; Savu D; Stutman D; Tanaka KA; Radu M; Doria D; Vasos PR Laser-driven Radiation: Biomarkers for Molecular Imaging of High Dose-rate Effects. Med. Phys. 2019, 46 (10). 10.1002/mp.13741.

(84). Qin H; Zhang V; Bok RA; Santos RD; Cunha JA; Hsu I-C; Santos BS,JD; Lee JE; Sukumar S; Larson PEZ; Vigneron DB; Wilson DM; Sriram R; Kurhanewicz J Simultaneous Metabolic and Perfusion Imaging Using Hyperpolarized 13C MRI Can Evaluate Early and Dose-Dependent Response to Radiation Therapy in a Prostate Cancer Mouse Model. Int. J. Radiat. Oncol. 2020, 107 (5), 887–896. 10.1016/j.ijrobp.2020.04.022.

(85). Golman K; Zandt R. i.; Lerche M; Pehrson R; Ardenkjaer-Larsen JH Metabolic Imaging by Hyperpolarized 13C Magnetic Resonance Imaging for In Vivo Tumor Diagnosis. Cancer Res. 2006, 66 (22), 10855–10860. 10.1158/0008-5472.CAN-06-2564. [PubMed: 17108122]

(86). Rodrigues TB; Serrao EM; Kennedy BWC; Hu D-E; Kettunen MI; Brindle KM Magnetic Resonance Imaging of Tumor Glycolysis Using Hyperpolarized 13C-Labeled Glucose. Nat. Med. 2014, 20 (1), 93–97. 10.1038/nm.3416. [PubMed: 24317119]

(87). Keshari KR; Wilson DM; Chen AP; Bok R; Larson PEZ; Hu S; Criekinge MV; Macdonald JM; Vigneron DB; Kurhanewicz J Hyperpolarized [2– 13C]-Fructose: A Hemiketal DNP Substrate for In Vivo Metabolic Imaging. J. Am. Chem. Soc. 2009, 131 (48), 17591–17596. 10.1021/ja9049355. [PubMed: 19860409]

(88). Utsumi H; Hyodo F Free Radical Imaging Using In Vivo Dynamic Nuclear Polarization-MRI. In Methods in Enzymology; Elsevier, 2015; Vol. 564, pp 553–571. 10.1016/bs.mie.2015.08.009. [PubMed: 26477265]

(89). Saito K; Sail D; Yamamoto K; Matsumoto S; Blackman B; Kishimoto S; Brender JR; Swenson RE; Mitchell JB; Krishna MC Synthesis and Evaluation of 13C-Labeled 5–5-Dimethyl-1-Pyrroline-N-Oxide Aimed at in Vivo Detection of Reactive Oxygen Species Using Hyperpolarized 13C-MRI. Free Radic. Biol. Med. 2019, 131, 18–26. 10.1016/j.freeradbiomed.2018.11.013. [PubMed: 30471347]

(90). Franck JM; Kausik R; Han S Overhauser Dynamic Nuclear Polarization-Enhanced NMR Relaxometry. Microporous Mesoporous Mater. 2013, 178, 113–118. 10.1016/j.micromeso.2013.04.019. [PubMed: 23837010]

(91). Neudert O; Mattea C; Stapf S Molecular Dynamics-Based Selectivity for Fast-Field-Cycling Relaxometry by Overhauser and Solid Effect Dynamic Nuclear Polarization. J. Magn. Reson. 2017, 276, 113–121. 10.1016/j.jmr.2017.01.013. [PubMed: 28183023]

(92). Gizatullin B; Mattea C; Stapf S Overhauser DNP FFC Study of Block Copolymer Diluted Solution. Magn. Reson. Imaging 2019, 56, 96–102. 10.1016/j.mri.2018.09.005. [PubMed: 30219267]

(93). Luchinat C; Parigi G Nuclear Relaxometry Helps Designing Systems for Solution DNP on Proteins. Appl. Magn. Reson. 2008, 34 (3–4), 379–392. 10.1007/s00723-008-0116-6.

(94). Parigi G; Ravera E; Bennati M; Luchinat C Understanding Overhauser Dynamic Nuclear Polarisation through NMR Relaxometry. Mol. Phys. 2019, 117 (7–8), 888–897. 10.1080/00268976.2018.1527409.

(95). Halse ME; Callaghan PT A Dynamic Nuclear Polarization Strategy for Multi-Dimensional Earth's Field NMR Spectroscopy. J. Magn. Reson. 2008, 195 (2), 162–168. 10.1016/j.jmr.2008.09.007. [PubMed: 18926746]

(96). Lee S-J; Shim JH; Kim K; Yu KK; Hwang S Dynamic Nuclear Polarization in the Hyperfine-Field-Dominant Region. J. Magn. Reson. 2015, 255, 114–121. 10.1016/j.jmr.2015.04.004. [PubMed: 25955437]

(97). Yoder JL; Magnelind PE; Espy MA; Janicke MT Exploring the Limits of Overhauser Dynamic Nuclear Polarization (O-DNP) for Portable Magnetic Resonance Detection of Low γ Nuclei. Appl. Magn. Reson. 2018, 49 (7), 707–724. 10.1007/s00723-018-1014-1.

(98). Zotev VS; Owens T; Matlashov AN; Savukov IM; Gomez JJ; Espy MA Microtesla MRI with Dynamic Nuclear Polarization. J. Magn. Reson. 2010, 207 (1), 78–88. 10.1016/j.jmr.2010.08.015. [PubMed: 20843715]

(99). Miloushev VZ; Di Gialleonardo V; Salamanca-Cardona L; Correa F; Granlund KL; Keshari KR Hyperpolarized 13 C Pyruvate Mouse Brain Metabolism with Absorptive-Mode EPSI at 1 T. J. Magn. Reson. 2017, 275, 120–126. 10.1016/j.jmr.2016.12.009. [PubMed: 28061381]

(100). van Meerten SGJ; Tayler MCD; Kentgens APM; van Bentum PJM Towards Overhauser DNP in Supercritical CO2. J. Magn. Reson. 2016, 267, 30–36. 10.1016/j.jmr.2016.04.002. [PubMed: 27082277]

(101). Sharma M; Janssen G; Leggett J; Kentgens APM; van Bentum PJM Rapid-Melt Dynamic Nuclear Polarization. J. Magn. Reson. 2015, 258, 40–48. 10.1016/j.jmr.2015.06.007. [PubMed: 26225439]

(102). Cheng T; Capozzi A; Takado Y; Balzan R; Comment A Over 35% Liquid-State 13C Polarization Obtained via Dissolution Dynamic Nuclear Polarization at 7 T and 1 K Using Ubiquitous Nitroxyl Radicals. Phys. Chem. Chem. Phys. 2013, 15 (48), 20819. 10.1039/c3cp53022a. [PubMed: 24217111]

(103). Cheng T; Mishkovsky M; Bastiaansen JAM; Ouari O; Hautle P; Tordo P; van den Brandt B; Comment A Automated Transfer and Injection of Hyperpolarized Molecules with Polarization Measurement Prior to in Vivo NMR: Automated Injection Protocol for in Vivo Hyperpolarized NMR. NMR Biomed. 2013, 26 (11), 1582–1588. 10.1002/nbm.2993. [PubMed: 23893539]

(104). Jannin S; Comment A; Kurdzesau F; Konter JA; Hautle P; van den Brandt B; van der Klink JJA 140 GHz Prepolarizer for Dissolution Dynamic Nuclear Polarization. J. Chem. Phys. 2008, 128 (24), 241102. 10.1063/1.2951994. [PubMed: 18601309]

(105). Chen H-Y; Hilty C Implementation and Characterization of Flow Injection in Dissolution Dynamic Nuclear Polarization NMR Spectroscopy. ChemPhysChem 2015, 16 (12), 2646–2652. 10.1002/cphc.201500292. [PubMed: 26139513]

(106). Krajewski M; Wespi P; Busch J; Wissmann L; Kwiatkowski G; Steinhauser J; Batel M; Ernst M; Kozerke S A Multisample Dissolution Dynamic Nuclear Polarization System for Serial Injections in Small Animals: Multisample Dissolution DNP Polarizer for Small Animals. Magn. Reson. Med. 2017, 77 (2), 904–910. 10.1002/mrm.26147. [PubMed: 26900678]

(107). Kiswandhi A; Niedbalski P; Parish C; Ferguson S; Taylor D; McDonald G; Lumata L Construction and 13C Hyperpolarization Efficiency of a 180 GHz Dissolution Dynamic Nuclear Polarization System: A 180 GHz Dissolution DNP System. Magn. Reson. Chem. 2017, 55 (9), 828–836. 10.1002/mrc.4597. [PubMed: 28407455]

(108). Balzan R; Fernandes L; Comment A; Pidial L; Tavitian B; Vasos PR Dissolution Dynamic Nuclear Polarization Instrumentation for Real-Time Enzymatic Reaction Rate Measurements by NMR. J. Vis. Exp. 2016, No. 108, 53548. 10.3791/53548. [PubMed: 26967906]

(109). Golman K; Ardenkjaer-Larsen JH; Petersson JS; Mansson S; Leunbach I Molecular Imaging with Endogenous Substances. Proc. Natl. Acad. Sci. 2003, 100 (18), 10435–10439. 10.1073/pnas.1733836100. [PubMed: 12930896]

(110). Kiswandhi A; Niedbalski P; Parish C; Ferguson S; Taylor D; McDonald G; Lumata L Construction and 13C Hyperpolarization Efficiency of a 180 GHz Dissolution Dynamic Nuclear Polarization System: A 180 GHz Dissolution DNP System. Magn. Reson. Chem. 2017, 55 (9), 828–836. 10.1002/mrc.4597. [PubMed: 28407455]

(111). Thurber KR; Yau W-M; Tycko R Low-Temperature Dynamic Nuclear Polarization at 9.4 T with a 30 mW Microwave Source. J. Magn. Reson. 2010, 204 (2), 303–313. 10.1016/j.jmr.2010.03.016. [PubMed: 20392658]

(112). Bornet A; Milani J; Vuichoud B; Perez Linde AJ; Bodenhausen G; Jannin S Microwave Frequency Modulation to Enhance Dissolution Dynamic Nuclear Polarization. Chem. Phys. Lett. 2014, 602, 63–67. 10.1016/j.cplett.2014.04.013.

(113). Chen H-Y; Hilty C Implementation and Characterization of Flow Injection in Dissolution Dynamic Nuclear Polarization NMR Spectroscopy. ChemPhysChem 2015, 16 (12), 2646–2652. 10.1002/cphc.201500292. [PubMed: 26139513]

(114). Milani J; Vuichoud B; Bornet A; Miéville P; Mottier R; Jannin S; Bodenhausen G A Magnetic Tunnel to Shelter Hyperpolarized Fluids. Rev. Sci. Instrum. 2015, 86 (2), 024101. 10.1063/1.4908196. [PubMed: 25725861]

(115). Kou il K; Kou ilová H; Bartram S; Levitt MH; Meier B Scalable Dissolution-Dynamic Nuclear Polarization with Rapid Transfer of a Polarized Solid. Nat. Commun. 2019, 10 (1), 1733. 10.1038/s41467-019-09726-5. [PubMed: 30988293]

(116). Pinon AC; Capozzi A; Ardenkjær-Larsen JH Hyperpolarized Water through Dissolution Dynamic Nuclear Polarization with UV-Generated Radicals. Commun. Chem. 2020, 3 (1), 57. 10.1038/s42004-020-0301-6.

(117). Ji X; Bornet A; Vuichoud B; Milani J; Gajan D; Rossini AJ; Emsley L; Bodenhausen G; Jannin S Transportable Hyperpolarized Metabolites. Nat. Commun. 2017, 8 (1), 13975. 10.1038/ncomms13975. [PubMed: 28072398]

(118). Solido Sandra I.. Flow 1H Dynamic Nuclear Polarization Studies in Normal Liquids and Supercritical Fluid Carbon Dioxide, Virginia Polytechnic Institute and State University, 2002.

(119). Tsai KH; Dorn HC A Model for Establishing the Ultimate Enhancements (A∞) in the Low to High Magnetic Field Transfer Dynamic Nuclear Polarization Experiment. Appl. Magn. Reson. 1990, 1 (2), 231–254. 10.1007/BF03166157.

(120). Dorn HC; Glass TE; Gitti R; Tsai KH Transfer Of 1H And 13C Dynamic Nuclear Polarization from Immobilized Nitroxide Radicals to Flowing Liquids. Appl. Magn. Reson. 1991, 2 (1), 9–27. 10.1007/BF03166265.

(121). Gitti R; Wild C; Tsiao C; Zimmer K; Glass TE; Dorn HC Solid/Liquid Intermolecular Transfer of Dynamic Nuclear Polarization. Enhanced Flowing Fluid Proton NMR Signals via Immobilized Spin Labels. J. Am. Chem. Soc. 1988, 110 (7), 2294–2296. 10.1021/ja00215a047.

(122). Kerwood DJ; Bolton PH Low-Field NMR. J. Magn. Reson. 1969 1986, 68 (3), 588–592. 10.1016/0022-2364(86)90352-5.

(123). Wagner S; Dinesen TRJ; Rayner T; Bryant RG High-Resolution Magnetic Relaxation Dispersion Measurements of Solute Spin Probes Using a Dual-Magnet System. J. Magn. Reson. 1999, 140 (1), 172–178. 10.1006/jmre.1999.1811. [PubMed: 10479560]

(124). Redfield AG Shuttling Device for High-Resolution Measurements of Relaxation and Related Phenomena in Solution at Low Field, Using a Shared Commercial 500 MHz NMR Instrument. Magn. Reson. Chem. 2003, 41 (10), 753–768. 10.1002/mrc.1264.

(125). Grosse S; Gubaydullin F; Scheelken H; Vieth H-M; Yurkovskaya AV Field Cycling by Fast NMR Probe Transfer: Design and Application in Field-Dependent CIDNP Experiments. Appl. Magn. Reson. 1999, 17 (2–3), 211–225. 10.1007/BF03162162.

(126). Grosse S; Yurkovskaya AV; Lopez J; Vieth H-M Field Dependence of Chemically Induced Dynamic Nuclear Polarization (CIDNP) in the Photoreaction of N -Acetyl Histidine with 2,2'-Dipyridyl in Aqueous Solution. J. Phys. Chem. A 2001, 105 (26), 6311–6319. 10.1021/jp004582i.

(127). Reese M; Lennartz D; Marquardsen T; Höfer P; Tavernier A; Carl P; Schippmann T; Bennati M; Carlomagno T; Engelke F; Griesinger C Construction of a Liquid-State NMR DNP Shuttle Spectrometer: First Experimental Results and Evaluation of Optimal Performance Characteristics. Appl. Magn. Reson. 2008, 34 (3–4), 301–311. 10.1007/s00723-008-0131-7.

(128). Krahn A; Lottmann P; Marquardsen T; Tavernier A; Türke M-T; Reese M; Leonov A; Bennati M; Hoefer P; Engelke F; Griesinger C Shuttle DNP Spectrometer with a Two-Center Magnet. Phys. Chem. Chem. Phys. 2010, 12 (22), 5830. 10.1039/c003381b. [PubMed: 20461246]

(129). Akasaka K; Naito A; Nakatani H; Imanari M Construction and Performance of a Temperature-jump NMR Apparatus. Rev. Sci. Instrum. 1990, 61 (1), 66–68. 10.1063/1.1141901.

(130). Joo C-G; Hu K-N; Bryant JA; Griffin RG In Situ Temperature Jump High-Frequency Dynamic Nuclear Polarization Experiments: Enhanced Sensitivity in Liquid-State NMR Spectroscopy. J. Am. Chem. Soc. 2006, 128 (29), 9428–9432. 10.1021/ja0611947. [PubMed: 16848479]

(131). Joo C-G; Casey A; Turner CJ; Griffin RG In Situ Temperature-Jump Dynamic Nuclear Polarization: Enhanced Sensitivity in Two-Dimensional 13C– 13C Correlation Spectroscopy in Solution. J. Am. Chem. Soc. 2009, 131 (1), 12–13. 10.1021/ja805521y. [PubMed: 18942782]

(132). Breeds Edward. Novel Hardware for Temperaturejump DNP. Ph. D. thesis, University of Nottingham, 2018.

(133). Yoon D; Soundararajan M; Caspers C; Braunmueller F; Genoud J; Alberti S; Ansermet J-P 500-Fold Enhancement of in Situ 13C Liquid State NMR Using Gyrotron-Driven Temperature-Jump DNP. J. Magn. Reson. 2016, 270, 142–146. 10.1016/j.jmr.2016.07.014. [PubMed: 27490302]

(134). van Meerten SGJ; Janssen GE; Kentgens APM Rapid-Melt DNP for Multidimensional and Heteronuclear High-Field NMR Experiments. J. Magn. Reson. 2020, 310, 106656. 10.1016/j.jmr.2019.106656. [PubMed: 31812888]

(135). Prandolini MJ; Denysenkov VP; Gafurov M; Endeward B; Prisner TF High-Field Dynamic Nuclear Polarization in Aqueous Solutions. J. Am. Chem. Soc. 2009, 131 (17), 6090–6092. 10.1021/ja901496g. [PubMed: 19361195]

(136). Denysenkov VP; Prandolini MJ; Krahn A; Gafurov M; Endeward B; Prisner TF High-Field DNP Spectrometer for Liquids. Appl. Magn. Reson. 2008, 34 (3–4), 289–299. 10.1007/s00723-008-0127-3.

(137). Höfer P; Parigi G; Luchinat C; Carl P; Guthausen G; Reese M; Carlomagno T; Griesinger C; Bennati M Field Dependent Dynamic Nuclear Polarization with Radicals in Aqueous Solution. J. Am. Chem. Soc. 2008, 130 (11), 3254–3255. 10.1021/ja0783207. [PubMed: 18293980]

(138). Liu G; Levien M; Karschin N; Parigi G; Luchinat C; Bennati M One-Thousand-Fold Enhancement of High Field Liquid Nuclear Magnetic Resonance Signals at Room Temperature. Nat. Chem. 2017, 9 (7), 676–680. 10.1038/nchem.2723. [PubMed: 28644482]

(139). Denysenkov V; Prandolini MJ; Gafurov M; Sezer D; Endeward B; Prisner TF Liquid State DNP Using a 260 GHz High Power Gyrotron. Phys. Chem. Chem. Phys. 2010, 12 (22), 5786. 10.1039/c003697h. [PubMed: 20461255]

(140). Dubroca T; Smith AN; Pike KJ; Froud S; Wylde R; Trociewitz B; McKay J; Mentink-Vigier F; van Tol J; Wi S; Brey W; Long JR; Frydman L; Hill S A Quasi-Optical and Corrugated Waveguide Microwave Transmission System for Simultaneous Dynamic Nuclear Polarization NMR on Two Separate 14.1 T Spectrometers. J. Magn. Reson. 2018, 289, 35–44. 10.1016/j.jmr.2018.01.015. [PubMed: 29459343]

(141). Annino G; Villanueva-Garibay JA; van Bentum PJM; Klaassen AAK; Kentgens APM A High-Conversion-Factor, Double-Resonance Structure for High-Field Dynamic Nuclear Polarization. Appl. Magn. Reson. 2010, 37 (1–4), 851–864. 10.1007/s00723-009-0091-6.

(142). Jakdetchai O; Denysenkov V; Becker-Baldus J; Dutagaci B; Prisner TF; Glaubitz C Dynamic Nuclear Polarization-Enhanced NMR on Aligned Lipid Bilayers at Ambient Temperature. J. Am. Chem. Soc. 2014, 136 (44), 15533–15536. 10.1021/ja509799s. [PubMed: 25333422]

(143). Fuiiil Y; Ishikawa Y; Koizumi Y; Omija T; Ohya Ik.; Mitsudo S; Miura S; Yamamori H; Kikuchi H; Fukuda A Development of Millimeter-Wave Fabry-Perot Resonator for Simultaneous Electron-Spin and Nuclear-Magnetic Resonance Measurement at Low Temperatures. In 2018 43rd International Conference on Infrared, Millimeter, and Terahertz Waves (IRMMW-THz); IEEE: Nagoya, 2018; pp 1–2. 10.1109/IRMMW-THz.2018.8510295.

(144). Fedotov A; Kurakin I; Fischer S; Vogl T; Prisner TF; Denysenkov V Increased Flow Rate of Hyperpolarized Aqueous Solution for DNP-Enhanced MRI Achieved by an Open Fabry-Pérot Type Microwave Resonator; preprint; Hyperpolarization/Instrumentation, 2020. 10.5194/mr-2020-20.

(145). Nevzorov AA; Milikisiyants S; Marek AN; Smirnov AI Multi-Resonant Photonic Band-Gap/Saddle Coil DNP Probehead for Static Solid State NMR of Microliter Volume Samples. J. Magn. Reson. 2018, 297, 113–123. 10.1016/j.jmr.2018.10.010. [PubMed: 30380458]

(146). Ardenkjær-Larsen JH; Bowen S; Petersen JR; Rybalko O; Vinding MS; Ullisch M; Nielsen N Chr. Cryogen-free Dissolution Dynamic Nuclear Polarization Polarizer Operating at 3.35 T, 6.70 T, and 10.1 T. Magn. Reson. Med. 2019, 81 (3), 2184–2194. 10.1002/mrm.27537. [PubMed: 30357898]

(147). Cheng T; Gaunt AP; Marco-Rius I; Gehrung M; Chen AP; Klink JJ; Comment A A Multisample 7 T Dynamic Nuclear Polarization Polarizer for Preclinical Hyperpolarized MR. NMR Biomed. 2020, 33 (5). 10.1002/nbm.4264.

(148). Bornet A; Melzi R; Perez Linde AJ; Hautle P; van den Brandt B; Jannin S; Bodenhausen G Boosting Dissolution Dynamic Nuclear Polarization by Cross Polarization. J. Phys. Chem. Lett. 2013, 4 (1), 111–114. 10.1021/jz301781t. [PubMed: 26291221]

(149). Song C; Hu K-N; Joo C-G; Swager TM; Griffin RG TOTAPOL: A Biradical Polarizing Agent for Dynamic Nuclear Polarization Experiments in Aqueous Media. J. Am. Chem. Soc. 2006, 128 (35), 11385–11390. 10.1021/ja061284b. [PubMed: 16939261]

(150). Sauvée C, Rosay M, Casano G, Aussenac F, Weber RT, Ouari O, Tordo P. Highly Efficient, Water-Soluble Polarizing Agents for Dynamic Nuclear Polarization at High Frequency. Angew Chem Int Ed Engl 2013, 52 (41), 10858–10861. [PubMed: 23956072]

(151). Hu K-N; Yu H; Swager TM; Griffin RG Dynamic Nuclear Polarization with Biradicals. J. Am. Chem. Soc. 2004, 126 (35), 10844–10845. 10.1021/ja039749a. [PubMed: 15339160]

(152). Sauvée C; Rosay M; Casano G; Aussenac F; Weber RT; Ouari O; Tordo P Highly Efficient, Water-Soluble Polarizing Agents for Dynamic Nuclear Polarization at High Frequency. Angew. Chem. Int. Ed. 2013, 52 (41), 10858–10861. 10.1002/anie.201304657.

(153). Lund A; Casano G; Menzildjian G; Kaushik M; Stevanato G; Yulikov M; Jabbour R; Wisser D; Renom-Carrasco M; Thieuleux C; Bernada F; Karoui H; Siri D; Rosay M; Sergeyev IV; Gajan D; Lelli M; Emsley L; Ouari O; Lesage A TinyPols: A Family of Water-Soluble Binitroxides Tailored for Dynamic Nuclear Polarization Enhanced NMR Spectroscopy at 18.8 and 21.1 T. Chem. Sci. 2020, 11 (10), 2810–2818. 10.1039/C9SC05384K. [PubMed: 34084341]

(154). Ravera E; Shimon D; Feintuch A; Goldfarb D; Vega S; Flori A; Luchinat C; Menichetti L; Parigi G The Effect of Gd on Trityl-Based Dynamic Nuclear Polarisation in Solids. Phys. Chem. Chem. Phys. 2015, 17 (40), 26969–26978. 10.1039/C5CP04138D. [PubMed: 26403358]

(155). Lumata L; Merritt ME; Malloy CR; Sherry AD; Kovacs Z Impact of Gd3+ on DNP of [1–13C]-Pyruvate Doped with Trityl OX063, BDPA, or 4-Oxo-TEMPO. J. Phys. Chem. A 2012, 116 (21), 5129–5138. 10.1021/jp302399f. [PubMed: 22571288]

(156). Stevanato G; Kubicki DJ; Menzildjian G; Chauvin A-S; Keller K; Yulikov M; Jeschke G; Mazzanti M; Emsley L A Factor Two Improvement in High-Field Dynamic Nuclear Polarization from Gd(III) Complexes by Design. J. Am. Chem. Soc. 2019, 141 (22), 8746–8751. 10.1021/jacs.9b03723. [PubMed: 31117477]

(157). Orlando T; Dervi o lu R; Levien M; Tkach I; Prisner TF; Andreas LB; Denysenkov VP; Bennati M Dynamic Nuclear Polarization of 13C Nuclei in the Liquid State over a 10 Tesla Field Range. Angew. Chem. Int. Ed. 2019, 58 (5), 1402–1406. 10.1002/anie.201811892.

(158). Bennati M OT Overhauser DNP in Liquids on 13C Nuclei. eMagRes 2019, 8 (1).

(159). Levien M; Hiller M; Tkach I; Bennati M; Orlando T Nitroxide Derivatives for Dynamic Nuclear Polarization in Liquids: The Role of Rotational Diffusion. J. Phys. Chem. Lett. 2020, 11 (5), 1629–1635. 10.1021/acs.jpclett.0c00270. [PubMed: 32003568]

(160). Lingwood MD; Siaw TA; Sailasuta N; Abulseoud OA; Chan HR; Ross BD; Bhattacharya P; Han S Hyperpolarized Water as an MR Imaging Contrast Agent: Feasibility of in Vivo Imaging in a Rat Model. Radiology 2012, 265 (2), 418–425. 10.1148/radiol.12111804. [PubMed: 22996746]

(161). Vuichoud B; Bornet A; de Nanteuil F; Milani J; Canet E; Ji X; Miéville P; Weber E; Kurzbach D; Flamm A; Konrat R; Gossert AD; Jannin S; Bodenhausen G Filterable Agents for Hyperpolarization of Water, Metabolites, and Proteins. Chem. - Eur. J. 2016, 22 (41), 14696–14700. 10.1002/chem.201602506. [PubMed: 27546550]

(162). McCarney ER; Han S Spin-Labeled Gel for the Production of Radical-Free Dynamic Nuclear Polarization Enhanced Molecules for NMR Spectroscopy and Imaging. J. Magn. Reson. 2008, 190 (2), 307–315. 10.1016/j.jmr.2007.11.013. [PubMed: 18078772]

(163). Cheng T; Mishkovsky M; Junk MJN; Münnemann K; Comment A Producing Radical-Free Hyperpolarized Perfusion Agents for In Vivo Magnetic Resonance Using Spin-Labeled Thermoresponsive Hydrogel. Macromol. Rapid Commun. 2016, 37 (13), 1074–1078. 10.1002/marc.201600133. [PubMed: 27184565]

(164). Capozzi A; Cheng T; Boero G; Roussel C; Comment A Thermal Annihilation of Photo-Induced Radicals Following Dynamic Nuclear Polarization to Produce Transportable Frozen Hyperpolarized 13C-Substrates. Nat. Commun. 2017, 8 (1), 15757. 10.1038/ncomms15757. [PubMed: 28569840]

(165). Capozzi A; Patel S; Gunnarsson CP; Marco-Rius I; Comment A; Karlsson M; Lerche MH; Ouari O; Ardenkjaer-Larsen JH Efficient Hyperpolarization of U- 13C-Glucose Using Narrow-Line UV-Generated Labile Free Radicals. Angew. Chem. Int. Ed. 2019, 58 (5), 1334–1339. 10.1002/anie.201810522.

(166). Henstra A; Lin T-S; Schmidt J; Wenckebach W Th. High Dynamic Nuclear Polarization at Room Temperature. Chem. Phys. Lett. 1990, 165 (1), 6–10. 10.1016/0009-2614(90)87002-9.

(167). Kagawa A; Negoro M; Ohba R; Ichijo N; Takamine K; Nakamura Y; Murata T; Morita Y; Kitagawa M Dynamic Nuclear Polarization Using Photoexcited Triplet Electron Spins in Eutectic Mixtures. J. Phys. Chem. A 2018, 122 (50), 9670–9675. 10.1021/acs.jpca.8b09934. [PubMed: 30475617]

(168). Negoro M; Kagawa A; Tateishi K; Tanaka Y; Yuasa T; Takahashi K; Kitagawa M Dissolution Dynamic Nuclear Polarization at Room Temperature Using Photoexcited Triplet Electrons. J. Phys. Chem. A 2018, 122 (17), 4294–4297. 10.1021/acs.jpca.8b01415. [PubMed: 29652146]

(169). Kagawa A; Miyanishi K; Ichijo N; Negoro M; Nakamura Y; Enozawa H; Murata T; Morita Y; Kitagawa M High-Field NMR with Dissolution Triplet-DNP. J. Magn. Reson. 2019, 309, 106623. 10.1016/j.jmr.2019.106623. [PubMed: 31669795]

(170). Kouno H; Kawashima Y; Tateishi K; Uesaka T; Kimizuka N; Yanai N Nonpentacene Polarizing Agents with Improved Air Stability for Triplet Dynamic Nuclear Polarization at Room Temperature. J. Phys. Chem. Lett. 2019, 10 (9), 2208–2213. 10.1021/acs.jpclett.9b00480. [PubMed: 30933529]

(171). Kouno H; Orihashi K; Nishimura K; Kawashima Y; Tateishi K; Uesaka T; Kimizuka N; Yanai N Triplet Dynamic Nuclear Polarization of Crystalline Ice Using Water-Soluble Polarizing Agents. Chem. Commun. 2020, 56 (26), 3717–3720. 10.1039/D0CC00836B.

(172). Liu G; Liou S-H; Enkin N; Tkach I; Bennati M Photo-Induced Radical Polarization and Liquid-State Dynamic Nuclear Polarization Using Fullerene Nitroxide Derivatives. Phys. Chem. Chem. Phys. 2017, 19 (47), 31823–31829. 10.1039/C7CP06073D. [PubMed: 29171613]

(173). Schroeder FC; Gronquist M Extending the Scope of NMR Spectroscopy with Microcoil Probes. Angew. Chem. Int. Ed. 2006, 45 (43), 7122–7131. 10.1002/anie.200601789.

(174). Fratila RM; Velders AH Small-Volume Nuclear Magnetic Resonance Spectroscopy. Annu. Rev. Anal. Chem. 2011, 4 (1), 227–249. 10.1146/annurev-anchem-061010-114024.

(175). Lee JH; Okuno Y; Cavagnero S Sensitivity Enhancement in Solution NMR: Emerging Ideas and New Frontiers. J. Magn. Reson. 2014, 241, 18–31. 10.1016/j.jmr.2014.01.005. [PubMed: 24656077]

(176). Luchinat E; Banci L In-Cell NMR: A Topical Review. IUCrJ 2017, 4 (2), 108–118. 10.1107/S2052252516020625.

(177). Mousoulis C; Xu X; Reiter DA; Neu CP Single Cell Spectroscopy: Noninvasive Measures of Small-Scale Structure and Function. Methods 2013, 64 (2), 119–128. 10.1016/j.ymeth.2013.07.025. [PubMed: 23886910]

(178). Gökay O; Albert K From Single to Multiple Microcoil Flow Probe NMR and Related Capillary Techniques: A Review. Anal. Bioanal. Chem. 2012, 402 (2), 647–669. 10.1007/s00216-011-5419-z. [PubMed: 21969176]

(179). Guo J; Jiang D; Feng S; Ren C; Guo J M-NMR at the Point of Care Testing. ELECTROPHORESIS 2020, 41 (5–6), 319–327. 10.1002/elps.201900329. [PubMed: 31850534]

(180). Sahin Solmaz N; Grisi M; Matheoud AV; Gualco G; Boero G Single-Chip Dynamic Nuclear Polarization Microsystem. Anal. Chem. 2020, 92 (14), 9782–9789. 10.1021/acs.analchem.0c01221. [PubMed: 32530638]

(181). Keller TJ; Laut AJ; Sirigiri J; Maly T High-Resolution Overhauser Dynamic Nuclear Polarization Enhanced Proton NMR Spectroscopy at Low Magnetic Fields. J. Magn. Reson. 2020, 313, 106719. 10.1016/j.jmr.2020.106719. [PubMed: 32217425]
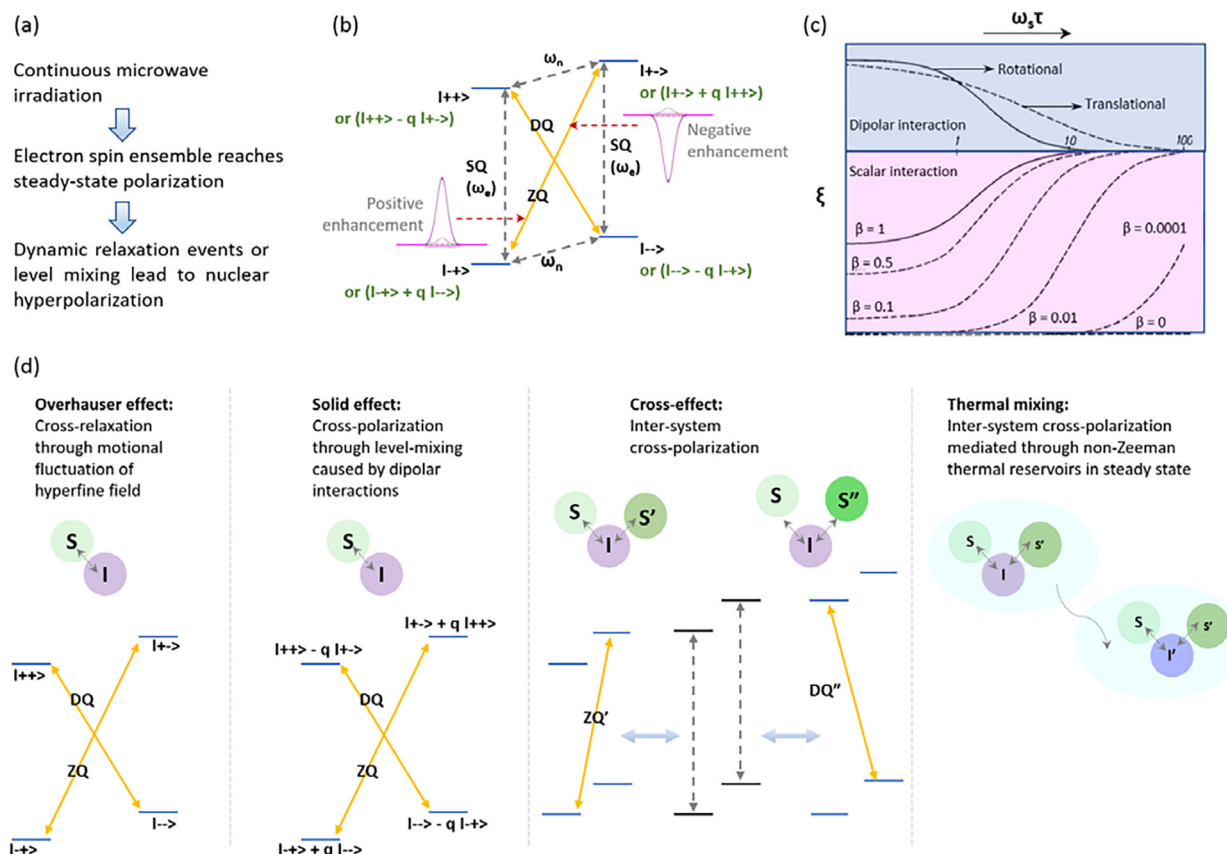
Figure 1:
Common features of continuous-wave dynamic nuclear polarization mechanisms. **(a)** Schematic of steps to produce a hyperpolarized nuclear ensemble using DNP under steady-state microwave irradiation. **(b)** Cartoon representation of eigen levels of an electron-nucleus (two-spin) system with S = ½ and I = ½. ω_e and ω_N are the allowed single quantum transitions (m_S (m_I) = ±1, m_I (m_S) = 0) It should be noted that the differences between electronic energy levels are at least three orders of magnitude larger than differences between nuclear energy levels, i.e. $\omega_e >>> \omega_N$. Dipolar and/or scalar components of the hyperfine interaction can facilitate the forbidden double quantum (DQ) and zero quantum (ZQ) transitions. Selectively driving either the DQ or ZQ transition leads to nuclear hyperpolarization. **(c)** Frequency/field-dependence of ODNP enhancement coupling factor (ξ) for modulation of dipolar and scalar components of HFI. (Adapted with permission from ref. 9 Copyright 1968 Elsevier) See text below for an explanation of the factor β. **(d)** Schematic of cross-polarization processes that lead to hyperpolarization in the four broad classes of mechanisms.
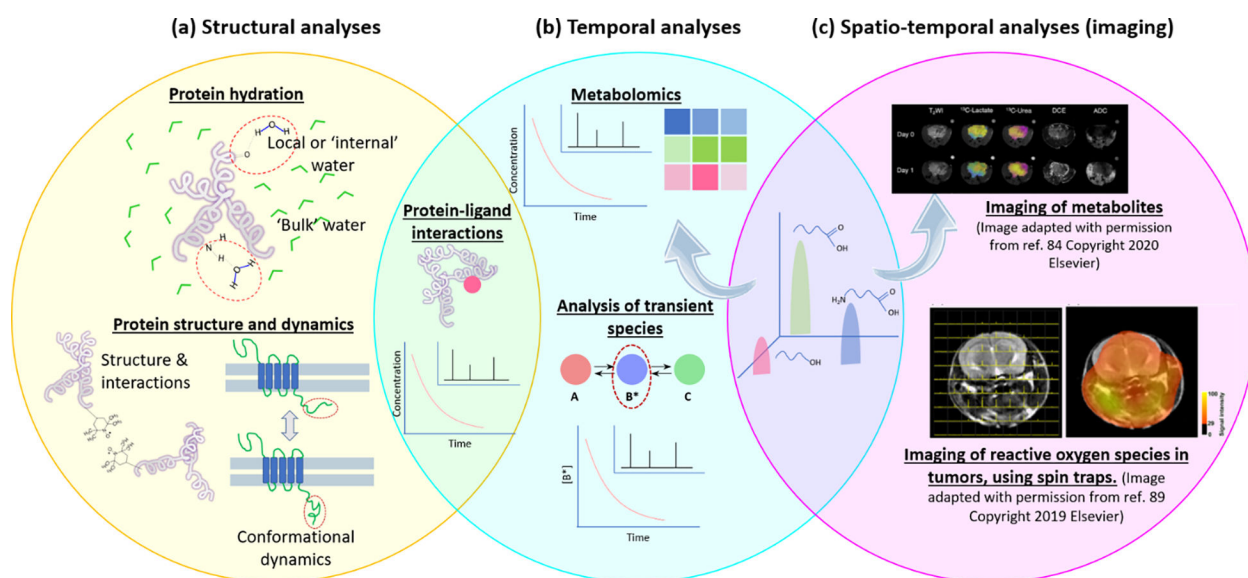
Figure 2:

Overview of current and potential future applications of liquid-state DNP NMR.
(a) Increasing the sensitivity of spectroscopic applications for structural studies; (b)
Spectroscopic identification of transient species such as reaction intermediates in solution;
(c) Imaging of species with low steady-state concentrations, e.g., metabolites and free
radicals at ambient temperature. The overlapping areas of the three circles show applications
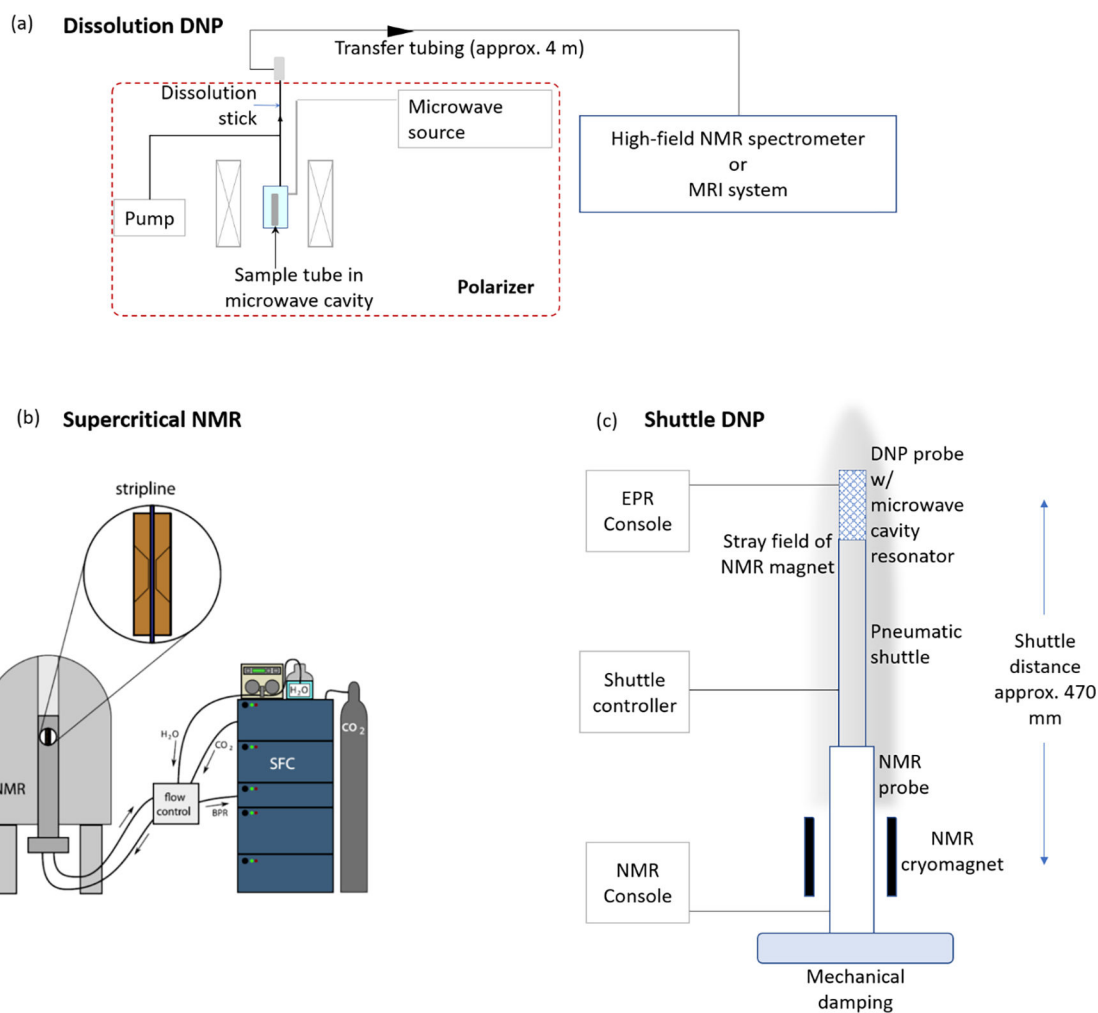that combine different types of studies.

Figure 3:

Summary of *ex situ* detection schemes. (a) Main components of a d-DNP setup. (b) Schematic of a supercritical NMR setup, which can be adapted for DNP by the addition of a microwave source and resonator. (Adapted with permission from ref. 100 Copyright 2016 Elsevier) (c) Main components of a shuttle-DNP setup.
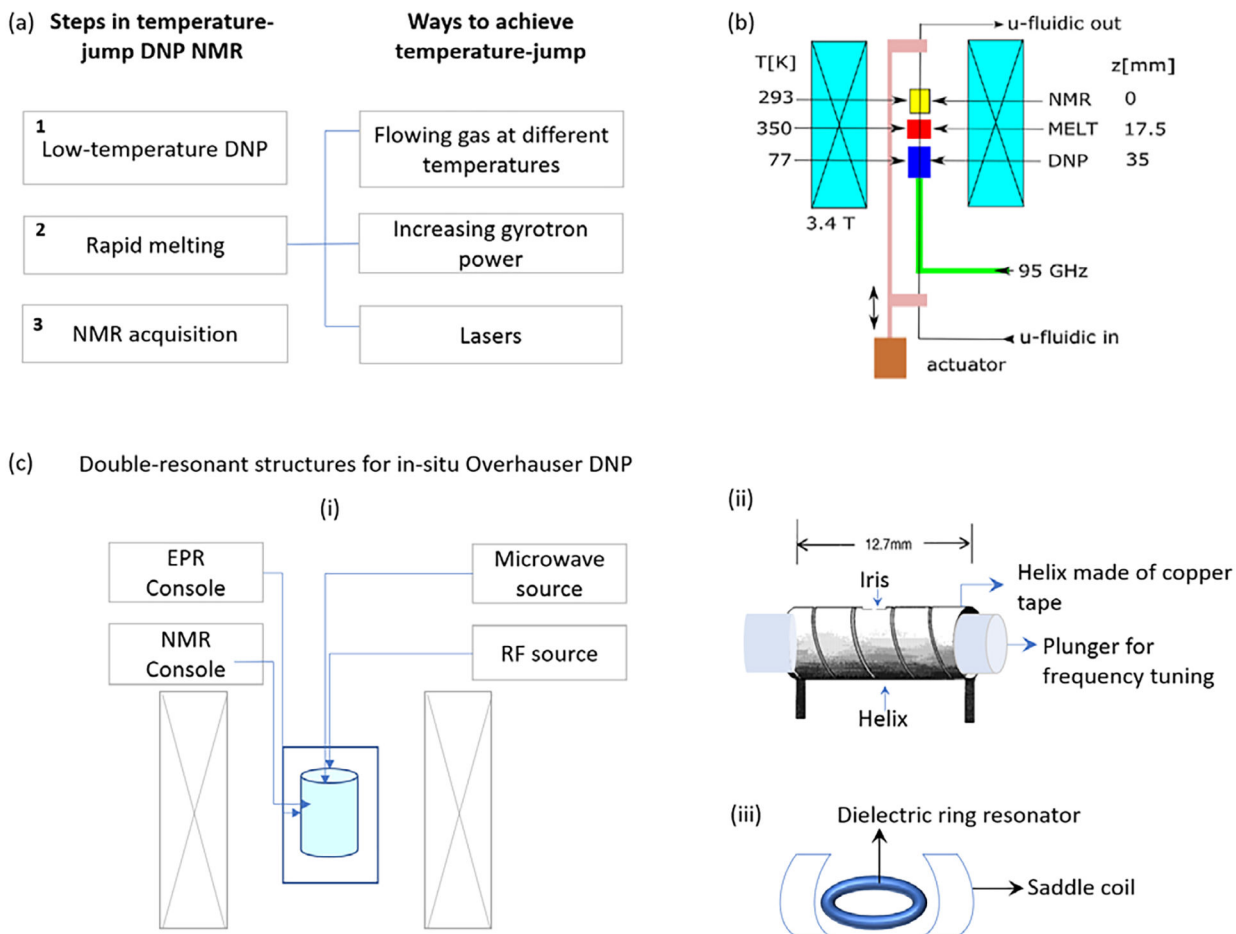
Figure 4:

Summary of *in situ* detection schemes. (a) Schematic of steps in temperature-jump NMR. The temperature can be produced using gas flow, microwave power from a gyrotron, or lasers. (b) Schematic of a rapid-melt apparatus consisting of microfluidic channels. Adapted with permission from ref. 101 Copyright 2015 Elsevier (c) i. Schematic of an *in situ* Overhauser setup where both DNP and NMR are conducted at the same magnetic field. To increase B_1 intensity, double resonant structures are used, for example: ii. a double-resonant flat helical cylinder (adapted with permission from *Weis et al. J. Magn. Res.* **140**, 293–299 Copyright 1999 Academic Press) or iii. a cylindrical resonator with matched ENDOR coils.
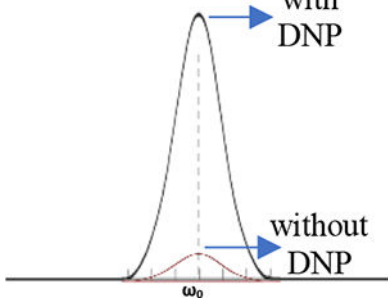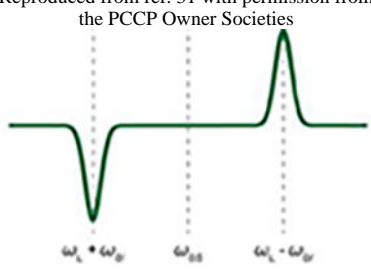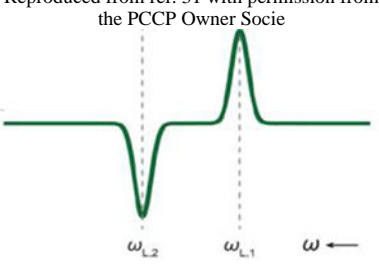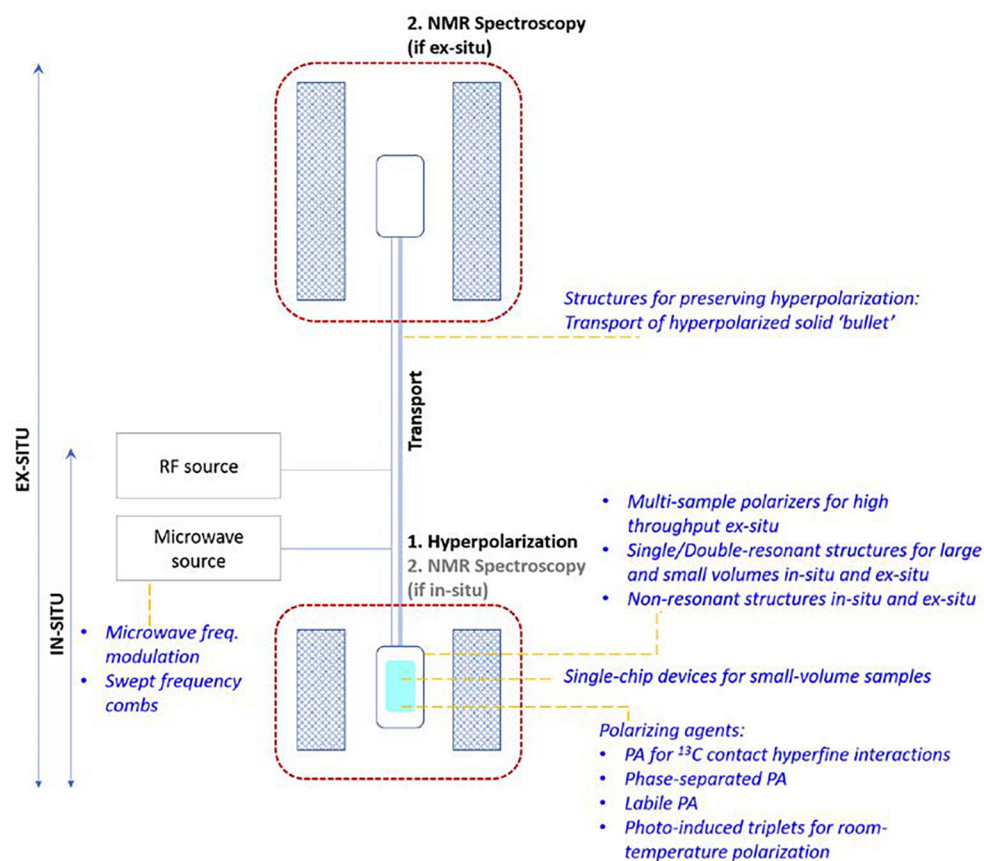
Figure 5:

Overview of future directions of research in liquid-state DNP NMR. The figure provides a simple schematic of the liquid-state DNP NMR setup, with possible areas of development for various components of the setup.

Table 1:

Summary of steady-state DNP mechanisms

	Overhauser effect	Solid effect[//]	Cross-effect[//]	
Typical frequency profile of DNP enhancement		Reproduced from ref. 31 with permission from the PCCP Owner Societies	Reproduced from ref. 31 with permission from the PCCP Owner Socie	
Observed in state	Liquid	Solid	Solid	
Detection schemes that apply mechanism	Direct detection, supercritical DNP	d-DNP, shuttle DNP, temperature-jump DNP, rapid-melt DNP	d-DNP, shuttle DNP, temperature-jump DNP, rapid-melt DNP	
Interactions leading to hyperpolarization	Relaxation through contact hyperfine, dipolar hyperfine interactions. Rate of fluctuation of electron density preferentially enables DQ or ZQ transition	Level mixing through dipolar hyperfine interaction, direct excitation of DQ or ZQ transition by microwaves	Dipolar electron-electron and dipolar hyperfine interactions; inter-system cross-coupling leads to cross-polarization from electron ensemble to nuclear ensemble	
Conditions	1. Saturating SQ transition: $\omega_{mw} = \omega_{SQ}$ 2. Relaxation through either ZQ or DQ: $\omega_{motion} \approx \omega_{ZQ/DQ}$	Selective, direct excitation of either ZQ or DQ transition: $\omega_{mw} = \omega_{SQ} \pm \omega_{0I}$. Requires PA with narrow EPR linewidths to achieve selectivity of DQ or ZQ transition.	$\omega_{mw} = \omega_{SQ}$ $\omega_e \gg \omega_N$; where ω_e is the width of the inhomogeneously broadened EPR line	

[//]B. Corzilius, *Phys. Chem. Chem. Phys.*, 2016, **18**, 27190 - Published by the PCCP Owner Societies